JPL PUBLICATION 81-6

Modeling Misregistration and Related Effects on Multispectral Classification

Fred C. Billingsley

April 15, 1981

National Aeronautics and
Space Administration

Jet Propulsion Laboratory
California Institute of Technology
Pasadena, California

JPL PUBLICATION 81-6

Modeling Misregistration and Related Effects on Multispectral Classification

Fred C. Billingsley

April 15, 1981

National Aeronautics and
Space Administration

Jet Propulsion Laboratory
California Institute of Technology
Pasadena, California

The research described in this publication was carried out by the Jet Propulsion Laboratory, California Institute of Technology, under contract with the National Aeronautics and Space Administration.

ABSTRACT

Misregistration is but one of a group of parameters (noise, class separability, spatial transient response, field sizes) affecting the accuracy of multispectral classifications. The entire group must be considered simultaneously. Any noise in the measurements (due to the scene, sensor, or to the analog/digital conversion) will cause a finite fraction of the measurements to fall outside of the classification limits, even within nominally uniform fields. For field boundaries, where the effects of misregistration are felt, additional pixels will be misclassified due to the mixture of materials in the pixels. Misregistration causes field borders in a given (set of) band(s) to be closer than expected to a given pixel, causing additional pixels to be misclassified. Simplified models of the various effects are used to gain conceptual understanding and to estimate the performance to be expected.

CONTENTS

Figures

Tables

SECTION 1

EXECUTIVE SUMMARY

INTRODUCTION

Spectral analysis generally takes the form of multispectral classification in which the classification is done by comparing the sample measurement vector to the statistics of the set of known material vectors (training statistics) representing all possible classes, and by using one of several decision methods, determining which of the knowns it most nearly matches.

The problem pursued will be the effects of misregistration on the accuracy of multispectral classification in answer to the question:

> What are the effects on multispectral classification accuracy of relaxing the overall scene registration accuracy from 0.3 to 0.5 pixel?

The misregistration is but one of a group of parameters (noise, class separability, spatial transient response, field size) which must all be considered simultaneously. The thread of the argument (which will be discussed in detail below) is this: any noise in the measurements (due to the scene, sensor, or the analog to digital process) causes a finite fraction of measurements to fall outside of the classification limits. For field boundaries, where the misregistration effects are felt, the misregistration causes the border in a given (set of) band(s) to be closer than expected to a given pixel, so that the mixed materials in the pixels causes additional pixels to fall outside of the class limits. Considerations of the transient distance involved in the difference in brightness between adjacent fields, when scaled to "per pixel", allows the estimation of the width of the border zones. The entire problem is then scaled to field sizes to allow estimation of the global effects.

This approach allows the estimation of the accuracy of multispectral classification which might be expected for field interiors, the useful number of quantization bits, and one set of criteria for an unbiased classifier.

CONCLUSIONS

The following briefly stated conclusions are developed in detail in the body of the report.

- The difference between 0.3 and 0.5 pixel misregistration is in the noise for multispectral classification.
- Precision users may have to reregister image segments anyway, making extreme registration precision by the system of less importance.
- Interpolation algorithm choice is relatively unimportant, provided a higher order interpolator is used.
- If small fields are important, small pixels are more important than sensor noise contributions.

In addition, several observations result:

- System registration to 1-2 pixels should satisfy users of film products.
- There is a grey area of 0.5 to 1-2 pixels in which the requirements for high precision are not well justified.

THE BASIC MODEL

The expected effect of misclassification may be estimated by a simple first-order approach, because the differences in classification accuracy between the many classification schemes and conditions that have been tested are overshadowed by the vagaries in the data and assumptions in the classification process, so that higher order analysis will contribute little additional understanding.

Consider first the probability of correct identification of a field interior pixel. Field interiors are nonuniform because of the combined effects of sensor noise, scaled to equivalent reflectivity ($N_E \Delta\rho$) and inherent nonuniformities in the field itself. The overall brightness distribution is considered to be Gaussian - this is approximately true for field interiors, although the distribution deviates considerably toward bimodal for mixed materials at field borders.

The combined effect of these various noise sources produces a finite probability of misclassification. (Figure S-1) The first-order estimate considers the total variance caused by the scene, sensor and quantization as compared to the defined class size limits, however these are determined. Similar, but relatively second-order, effect may be expected with a higher order analysis. Proper classifier training, resulting in accurate limits, is essential (Hixson et al, 1980).

For simplicity, and because of the later desire to misregister one (or more) of the bands, the discussion will assume that spectral bands as sensed will be used, and that for recognition, the unknown pixel must fall between

appropriate limits in every band tested. Therefore, brightness outside of a limit in any one band is sufficient for rejection, so that we need to consider only one band at a time.

The probability of a sample being within the class limits can be derived by assuming that an ensemble of clean signals from a series of areas of the same material can be anywhere within the quantizing range with uniform probability, but that individual samples are perturbed by the Gaussian noise with a distribution equal to σ. The probability distribution of the signal plus noise is found by convolving the probability distribution of the signal with that of the noise. The probability of correct class assignment (i.e., the pixel is within the class limits) is then found by integrating the probability distribution between appropriate class limits (Friedman 1965). The result of this calculation is shown in Figure 5-2. In the useful range of β ($3 < \beta < 7$), the curve can be approximated by

$$\beta \log P = -0.40$$

where P = probability of correct classification, and

$$\beta = \frac{\text{class size}}{\sigma_{\text{scene}}}$$, with class size and σ_{scene} in the same units.

Sources of noise will be the scene itself and the sensor, both assumed to be random for this analysis. The root mean square (rms) sum is taken to give the total effective noise. A number of pixel measurements may be averaged together to reduce the noise before classification. This final noise figure may be compared to the width of the class to give β, from which the probability P of correct classification may be estimated. This leads to the Classification Error Estimator, Fig. 5-3.

As an example, consider a scene having a field-interior variation of 3%, to be viewed with a sensor having a total noise figure of 1%. The total effective noise seen by the classifier (upper left) will be the rms sum of these, or 3.16%, which for a total 0-255 digital number (dn) range, would be 8.1 dn. If the class width (determined by the classifier algorithm) is 25 dn (right center) the $\beta = 3.1$, giving $P = 0.742$ (right lower). If this P is not accurate enought for the analysis, several pixels must be averaged(right upper): a 2x2 averaging will raise β to 6.2, giving a new $P = 0.86$.

Considering β in this way allows an estimation of the total noise permissible as it affects the attainable classification accuracy. If the amount of scene noise to be encountered in a given classification task can be estimated, the allowable extra noise from the sensor and quantization can be specified by estimating the loss of accuracy of the classification caused by quantization error. This leads to an estimate of the number of bits which will be useful.

Define the perfect sensor as having no random noise nor quantization error (i.e., an infinite number of bits). This will define (for nxn pixels averaged)

$$\beta = \frac{\text{class size} \cdot n}{\sigma_{\text{scene}}} \quad \text{and} \quad P_o = 10^{-0.4/\beta_o} ,$$

For the real sensor, $\beta<\beta_o$ because of the finite σ_{sensor} and $\sigma_{quantization}$.

The new probability of correct classification P is related to P_o by:

$$P = P_o^{(\beta/\beta_o)}$$

A plot of the loss in classification accuracy vs. P_o is given in Figure S-4, for the parameter families β_o/β and $\sigma_{sensor}/\sigma_{scene}$. Noise allocation starts with defining of the desired P_o and ascertaining that the required β_o can be obtained. Definition of the allowed ΔP determines (e.g., from the graph) the allowed $\sigma_{sensor}/\sigma_{scene}$. An estimation of the scene noise for which the other conditions apply allows the calculation of the total sensor noise allowed. The final step is to partition this noise between sensor random noise and quantization noise.

For example, let the desired P_o = 85% and allow no more than 2% loss due to the total sensor noise. The no-sensor-noise β_o must be ≥ 5.7 to give P_o. Then, from Figure S-4, the allowed $\sigma_{sensor} = 0.6 \times \sigma_{scene}$. If the scene has a σ_{scene} = 2%, the allowable σ_{sensor} = 0.6x2% = 1.2%, which must be partitioned between $NE\Delta\rho$ and the quantization noise. For $NE\Delta\rho$ = 1%, the allowable $\sigma_{quant} = \sqrt{1.2^2 - 1^2}$ = 0.66%, which can be met by 6-bit quantization.

Two observations are important here: (1) Increasing the number of bits of quantization produces improvements which asymptotically approach zero, as each successive bit reduces the step size by a factor of 1/2. (2) A scene having as little as 2% variation is a very uniform scene. Since this noise is rms'd with the sensor noise, it will overwhelm any but a very noisy sensor. Therefore, for purposes of multispectral classification, more than six bits would seem to be unnecessary.

EDGE EFFECTS

To this point, the analysis is based on pixels well inside uniform fields and well away from field boundaries. A number of experimenters have spent appreciable time discovering that classification accuracy falls off at boundaries due to what has become known as the mixed-pixel effect. We will start at that point and attempt to model the effect to allow us to quantify our expectations.

We assume as a starting point that all the spectral bands used in classification, whether obtained from one date or series of dates, are in perfect registration. This means that when the pixel grids from each band are aligned the data contents (field borders, roads, all features) are also aligned - note that this is more than simply having all internal distortions removed, which is all that most geometric rectifications accomplish. Misregistration will (later) be considered as the lack of alignment of the pixel grids; because the computer can only work with pixel grids, aligning these pixel grids appears to the computer as a shift in the boundaries. We will assume that training samples are accurate and that class limits have been set from these by the classifier chosen. The classification is modelled as follows: signature shifting in any individual band will tend to cause misclassification, so that the situation may be treated one band at a

time. The effects of pixel mixture in all bands may then be rms'd together if desired. The entire analysis simplifies to the consideration of the transient intensity shift across field boundaries as compared to the class limits and the noise components of the measurement.

The first step in analyzing the spatial extent of pixel mixing across borders is to estimate the shape and extent of the transient intensity shift. If the impulse response functions or the modulation transfer functions (MTFs) of the various components (and, hence, the entire system) are known, a precise transient response may be calculated. For example, the specifications for the Thematic Mapper for Landsat D call for a 2% to 98% time equivalent of about 2 pixels implying a 10%-90% transient response of about 1.3 pixel. The practical result of this is that the "infinitely sharp" edges of the real scene will be softened by the filtering effect of the scanning aperture (assumed to be rectangular and having uniform response) and it is this softened transient response which is sampled. Interpolation required for registration will cause some further softening, and the use of any of the competent higher-order interpolation functions (sinx/x, TRW cubic convolution, modified cubic convolution, other splines) will have minor effects of the rise time. A total T_{10-90} (transient response from 10% to 90%) of 1.5 pixels with no ringing will be used as a surrogate global value.

The transient situation across a border is sketched in Fig. S-5. We are concerned here with the decrease in probability that a given pixel will have a value within the class limits as that pixel moves toward the boundary, as shown in Figure S-6. The analysis only needs to determine the area under the normal curve (assuming the noise is Gaussian) between the limits as determined by the classification class size and the offset from the "field interior value" caused by the mixture. The important scaling involved is the amount of signal shift caused by the transient total shift T, as related to the desired class size S, for a given β. The left portion of Figure S-7 reflects this shift in brightness (vertical axis) as it affects the area within the class (the probability of recognition).

The transient rise distance estimated for the Thematic Mapper has very close to a Gaussian shape and a $T_{10-90} = 1.5$ pixel. The amount of brightness shift is the difference between the brightness of the field under consideration and the adjacent field which is causing the shift. The important intensity relation is the magnitude of this shift, T, as related to the size S of the class being tested by the ratio T/S. These curves, for various T/S, are combined with the probability curves of the previous discussion in Figure S-7. From this may be estimated the loss in probability in classification of pixels near borders.

BIAS IN FIELD SIZE ESTIMATION

It can be appreciated that several things are happening simultaneously: If the lower limit of field B and the upper limit of field A have a gap between, pixels "lost" by field B will not be picked up by field A, and will be considered unknowns and not be counted in either field. The lost pixels will be some interior pixels, due to insufficient β, and a large number of near-border pixels, resulting in apparent field size loss. Only if the lower limit of field B and the upper limit of field A are coincident will pixels lost from one field be picked up by the other, and vice versa, to give

complete account of all pixels. For the field size estimator to be unbiased, the loss nd-pickup in both directions must cancel; that is, on the average the true border must be located. The total effect will depend on the ratio of the number of border pixels to the number of field-interior pixels, and hence is a function of the field shape and size.

This leads directly to the required algorithm for field size estimation: First divide the scene into blobs, each of which is sufficiently uniform, and with closed boundaries. Then for each blob (field) determine the average brightness for all the interior pixels which are safely away from the border. For each segment of the border, the correct field edge decision level is midway (in σ's) between the average brightness of the two fields on either side. After the borders are located using this criterion, the field interiors may be reclassified using the classification limits as determined from the training samples.

EFFECTS OF MISREGISTRATION

In preparation for estimation of the misregistration effects, an analysis will first be made of the expectations of registered data and the sensitivity to the various parameters estimated. The starting model used has rectangular fields aligned with the pixel grid. Pixels are grouped into four zones: 1) Interior (i)-those with centers 2 or more pixels inside borders, 2) Inner border (ib)-pixels with centers 1-1/2 pixel inside borders, 3) Outer border (ob)-pixels with centers 1/2 pixel inside borders, 4) Exterior border (xb)-pixels outside the borders, with centers 1/2 pixel outside. Estimates of classification accuracy for each zone are obtained from Figure S-7. The total estimate of classification accuracy is the sum of pixels in each zone multiplied by the corresponding zone accuracy estimate. Later, the field will be misregistered, changes in the number of pixels in each zone calculated, and the probabilities again summed. The following parameters are required:

- r - the field shape ratio, length of long side/length of short side
- T - transient brightness difference between field being considered and its neighbor
- S - decision class size
- τ - transient distance for 10% to 90% response
- β - class size S/σ of Gaussian noise

The following global values selected for the parameters are considered to be representative:

$r = 2$
T/S = 1 to 5
τ = 1.5 pixels
β = 3 to 5

After the parameters r, T/S, τ , and β are selected, the resultant (from Fig. S-7) probabilities are substituted for the brightnesses in the various zones to produce a "probability image" aligned with the desired output pixel grid. The probability assigned to a pixel at a given location represents the probability that that pixel will have a brightness falling within the classification limit determined by the classifier, for the given spectral

band. The total probability of correct classification is given by

$$P = \frac{1}{cn_1^2}\left[p_i n_i + p_{ib} n_{ib} + p_{ob} n_{ob} + p_{xb} n_{xb}\right]$$

where n_1 is the field width (short side) in pixels, and n_i, n_{ib}, n_{ob}, n_{xb} are the number of pixels in the various zones. Using these values, the global estimate of the probability of correct classification with no misregistration is given Figure 5-8 for three values of T/S. The predominant effect is the pixel mixture (the effect of T/S). As expected, this is worst for small fields (n_1 small) because of the larger percentage of border pixels for these fields. Note that for T/S = 1, decision level midway between brightnesses of adjacent fields, no probability loss occurs, even with small fields. Unfortunately, this desirable condition cannot be systematically obtained.

MISREGISTRATION OF CONGRUENT FIELDS

The initial model for misregistration is a displacement of d pixels, equal in both x and y. The result of this misregistration is that some area is lost from the external border, causing a further classification accuracy decrease. The misregistration loss as seen by the external border loss is given by

$$\Delta P = p_{xb}\left[d\,\frac{r+1}{r}\,\frac{1}{n_1} + (4d - d^2)\frac{1}{n_1^2}\right]$$

The basic character of this misregistration loss term is $1/n_1$, so that it will have a slope approximately equal to -1 on a log-log plot vs n_1. The precise results depend critically on the values of p_{xb} estimated for the p_{xb} from Figure 5-7:

T/S	β	τ = 1	τ = 1.5	τ = 2
1	3	.10	.14	.20
	5	.02	.025	.07
	7	0	.01	.04
2	3	0	0	0
	5	0	0	0
	7	0	0	0

Using these values, the loss ΔP due to displacement misregistration is plotted in Figure 5-9 for various parameter combinations.

MISREGISTRATION DUE TO NONCONGRUENCE

1. SIZE AND RATIO (ASPECT) CHANGES

Size and aspect ratio changes can come about from several causes such as scan velocity or altitude changes, and if uncompensated can cause additional

misregistration errors. Progressive misregistration from a point of accurate registration will be caused by both causes (Figure S-10a); the modeling of this effect considers first that size changes $N = n'/n$ will cause a shift in points n to points n' both vertically and horizontally, and then that changes in aspect ratio will cause further shifts in the horizontal position of vertical borders by changing the field shape ratios by the factor $R = r'/r$. The resulting shifts are:

$$\Delta n_v = (N - 1)\, n_v \quad \text{and} \quad \Delta n_h = (NR - 1)\, r n_v$$

For analysis, this shift will be divided around the borders symmetrically as optimum field registration is accomplished (Figure S-10b). Two cases must be distinguished (using scan velocity as a surrogate cause):

Case I: A slow scan decreases pixel spacing and puts more pixels into a given field. When these are placed into the output grid, the field appears stretched. The field as defined by the other (correct) bands now covers only part of the stretched field, so that the classification tends to see only interior pixels, and the accuracy will increase, ultimately reaching the field-interior accuracy. The sizes of the border errors are:

$$e_1 = \frac{1}{2}(N - 1)\, n_1 \quad \text{and} \quad e_2 = \frac{1}{2}(NR - 1)\, r n_1$$

Case II: A fast scan has the opposite effect, causing the field to appear smaller and the analysis pixels defined by the other bands now include more exterior pixels. The classification accuracy will decrease.

For fast scan, the smaller apparent field covers an area expressed as a fraction f_i of the total:

Fractional Areas:

$$f_i = \frac{r'(n_1')^2}{r n_1^2} = RN^2 \qquad \text{(Interior)}$$

$$f_{xb} = \frac{2Nn_1 + 2NRn_1 r + 4}{r n_1^2} \qquad \text{(External Border)}$$

The total expected probability is

$$P_{tot} = f_i P_i + f_{xb} P_{xb} \ .$$

Since the external border pixels are now included within the analyzed field, but with a low probability, the fractional area RN^2 represents approximately the fraction of the basic field-interior accuracy to be expected. Since the total size shrinkage (in pixels) is small for small n_1, only larger n_1 need be considered, and the $1/n_1^2$ term may be dropped.

This allows P_{tot} to be approximated for r = 2 by:

$$P_{tot} \approx RN^2 p_i + \frac{3}{n_1} p_{xb}$$

For large fields, the probability is seen to be independent of field size, and only weakly dependent (because of low p_{xb}) for small sizes.

2. WAVY BORDERS AND MULTIPLE ACQUISITIONS

For single-band analysis, with borders distorted so that there are pixels both inside and outside of the analyzed area, some pixels will have increased probabilities of correct classification and some will have less. The decrease in probability across border is (very) approximately linear, so that the (signed) average displacement will model the effect.

For multiband analysis, those pixels having a low probability of classification will have the largest effect as the net probability at each pixel location is the product of the probabilities obtained for each acquisition (band). In this case the rms displacement will produce a better model of the effects.

SOME OBSERVATIONS

1. ON BASIC CLASSIFICATION

- The total noise figure (compared to the class size in a given determination) controls β, and in turn controls the maximum attainable classification accuracy. However, for practical range of $3 < \beta < 7$, increasing β has only a moderate effect.
- Because of this, if small fields are most important, the reflected energy might more profitably be divided into smaller pixels, even at the expense of $NE\Delta\rho$. As this will cause an increase in data rate, optimum coding should be investigated. The possible noise introduced in reconstructing the data will cause some further decrease in the overall effective $NE\Delta\rho$ and so decreases β. But since there is smaller sensitivity to β than to $1/n_1$, there should be a net gain in utility.
- Increasing the number of bits of quantization produces improvements which asymptotically approach zero, as each successive bit reduces the step size by a factor of 1/2.
- A scene having as little as 2% variation is a very uniform scene. Since this noise is rms'd with the sensor noise, it will overwhelm any but a very noisy sensor. Therefore, for purposes of multispectral classification, an extreme number of bits would seem to be unnecessary.

2. ON EDGE EFFECTS

- For accurate field size estimation, the decision brightness must be halfway between the brightnesses of the fields on either side of a given boundary. This means that classifiers set for material identification will in general produce errors in field size. But the

field-interior brightness is increasingly hard to estimate for small fields because of the fewer interior pixels.

- It is important to keep the transient response distance and the accompanying sample spacing small, to get as many pixels into a given ground distance as possible. Field area errors become large at $n_1 = 5$ or less. The transient distance must also be matched between spectral bands.
- At the resolution expected for the Thematic Mapper, the atmospheric point spread function may become more dominant than the Thematic Mapper point spread function. If this is determined to be true, the registration requirements may be relaxed since scene-dependent registration will be required anyway.

3. ON MISREGISTRATION

- For large T/S (i.e., 2 or more) the edge effects are so great that the base probability is drastically affected, and the external border pixels have zero probability of being within the class limits. For this reason, there is no misregistration effect for large T/S.
- Square fields show the most misregistration loss, when scaled to n_1.
- A shape ratio r=2 is believed to be representative.
- Misregistration loss decreases with higher β. However, these losses in general are small to begin with, and the discussion calling for sacrifice of β to gain smaller IFOV (more pixels n_1 into a given field) would seem to override.
- Increase in τ decreases the basic accuracy of edge pixels and also increases the misregistration losses.
- Geometric rectification and registration procedures must not only remove the internal distortions but must also produce pixels on a defined (preferably ground-referenced) grid. Current procedures do not do this. Without this reference grid, users will have to reinterpolate before multi-temporal data can be compared.
- Scale and aspect ratio errors will have only minor effects on moderate-area problems. But they will cause problems in correlating over large distances.
- Altitude relief displacement will require users to use many control points to register images in areas of high relief.
- Unless standard reference grids are established, users requiring registration will have to interpolate every image, even in low relief areas.
- For single-band analysis, the algebraic average of the displacement may be used. For multiband analysis, with erratic errors in location among the bands, the lowest probability of correct classification holds and the rms of the displacements is appropriate.

AN UNANSWERED QUESTION

This report models the potential misregistration effects on multispectral classification accuracy. It may allow the comparison of the various tests and simulations, and points out the variables which must be reported for those simulations to allow their validation. It does not answer the following question: Given a certain loss in accuracy due to misregistration, how does that damage the ability to use the data analysis results? These evaluations will be discipline dependent, and must be sought separately.

REFERENCES

1-1 Friedman, H.D., On the Expected Error in the Probability of Misclassification, Proc IEEE Vol 53, p. 658.

1-2 Hixson, M., Scholz, D., Fuhs, N., Akiyama, T., Evaluation of Several Schemes for Classification of Remotely Sensed Data, Photogrammetric Engineering and Remote Sensing, Vol 46 # 12, Dec 1980, pp 1547-1553.

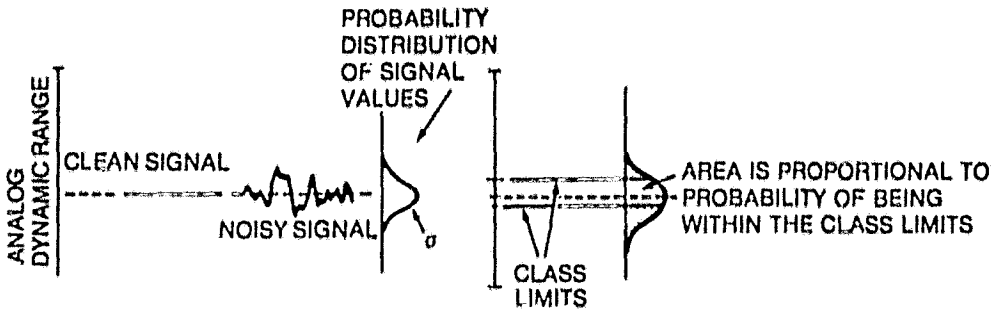

Figure S-1 Effect of Noise on the Probability of Correct Multi-spectral Classification

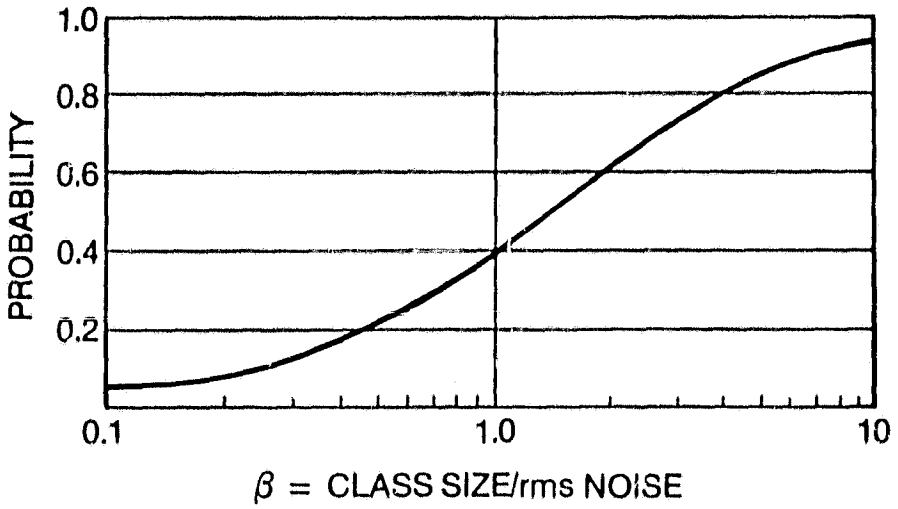

Figure S-2 Given a Signal Uniformly Probable over the Dynamic Range, and Gaussian Noise with standard Deviation = σ . The curve shows the Probability of Correctly Recognizing a class corresponding to the Noise-free Signal as a Function of the Ratio β = class size / σ .

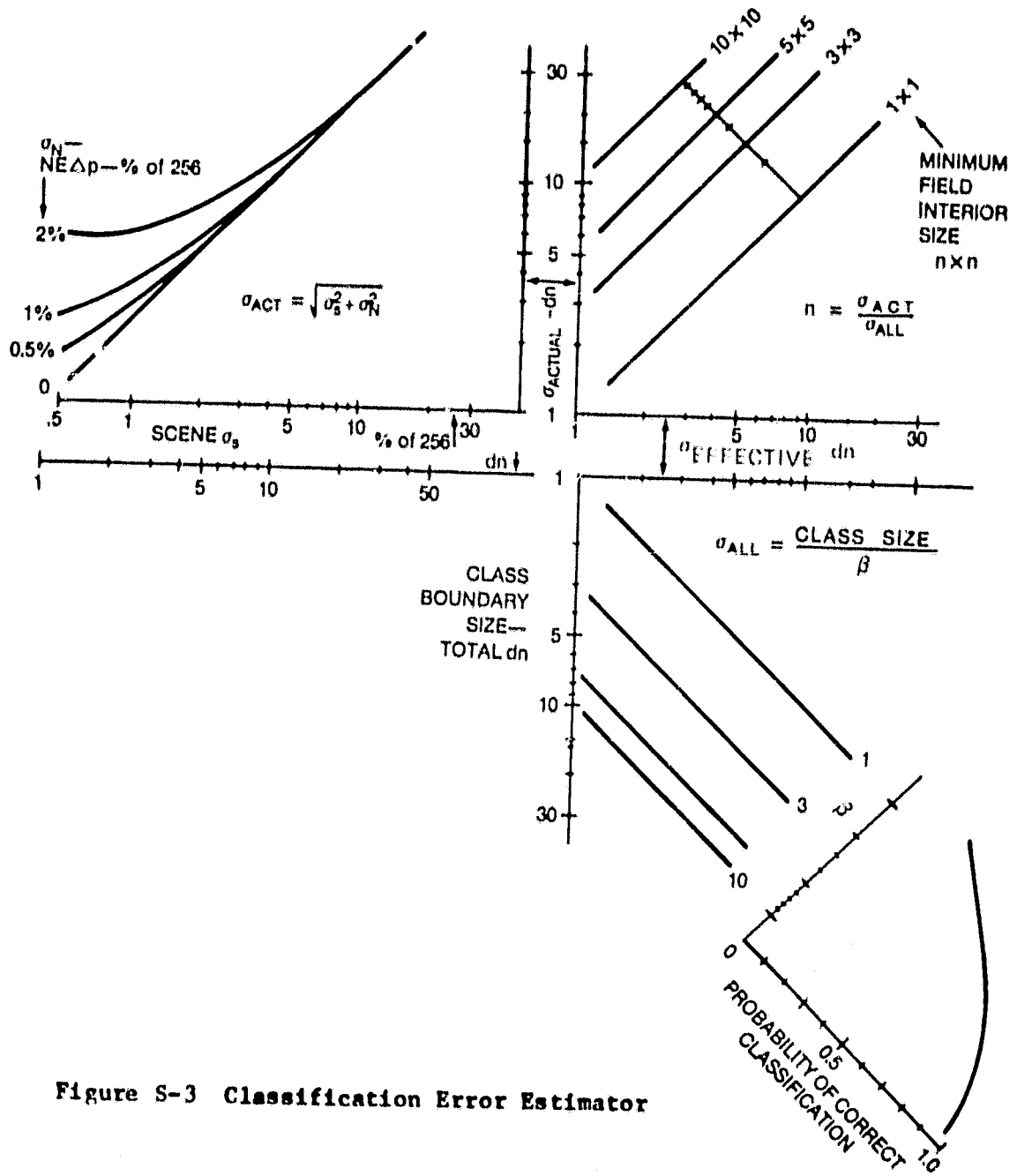

Figure S-3 Classification Error Estimator

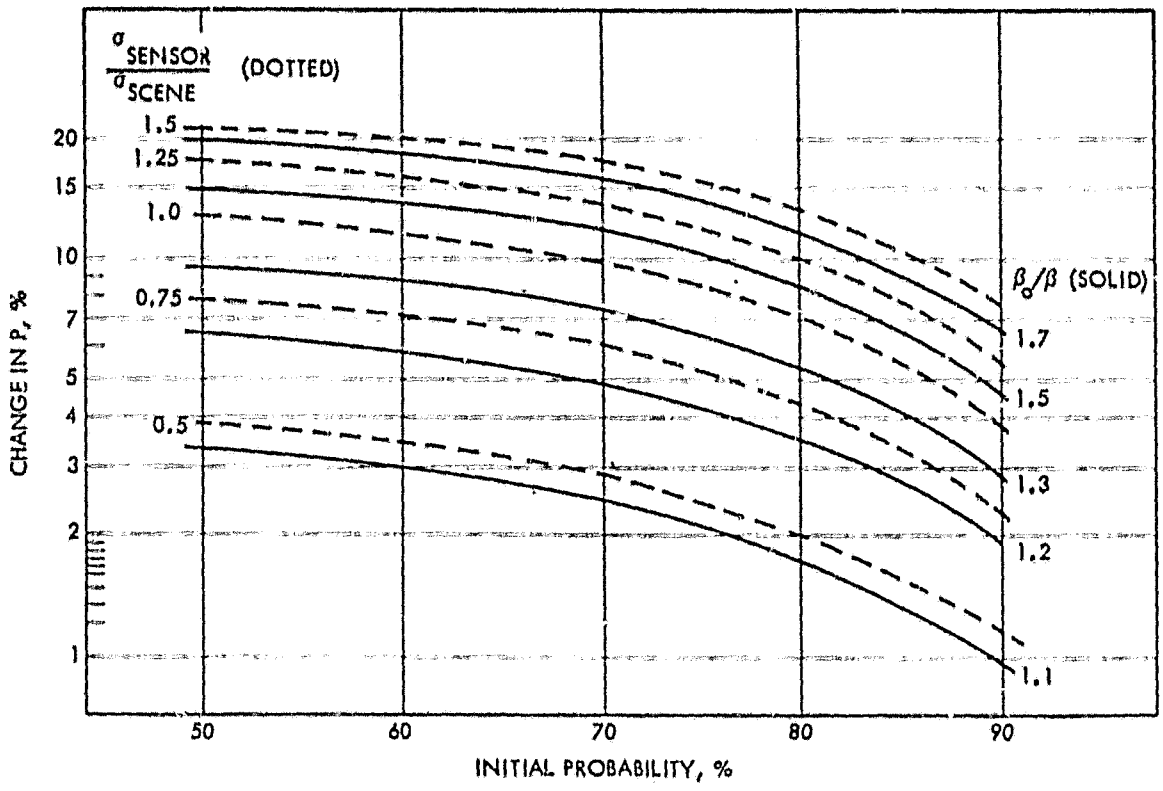

Figure S-4 Loss in Classification Accuracy due to Noise

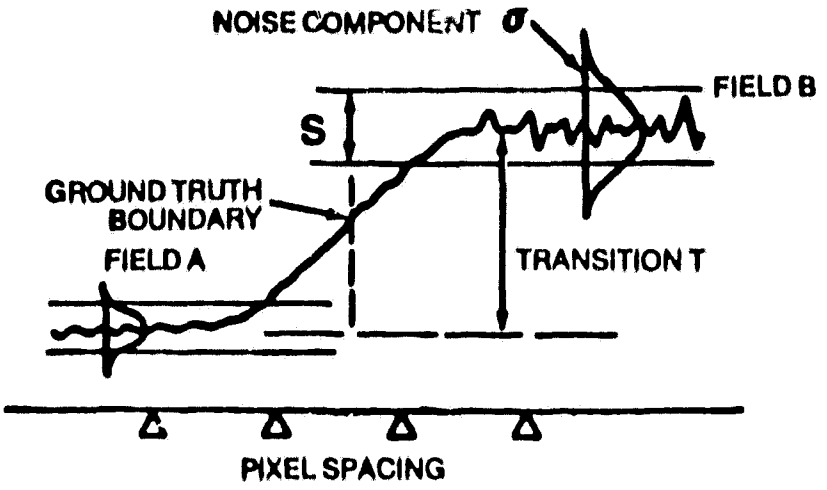

Figure S-5 Cross Section of brightness trace across a boundary between two fields, showing the distance required for the brightness transition.

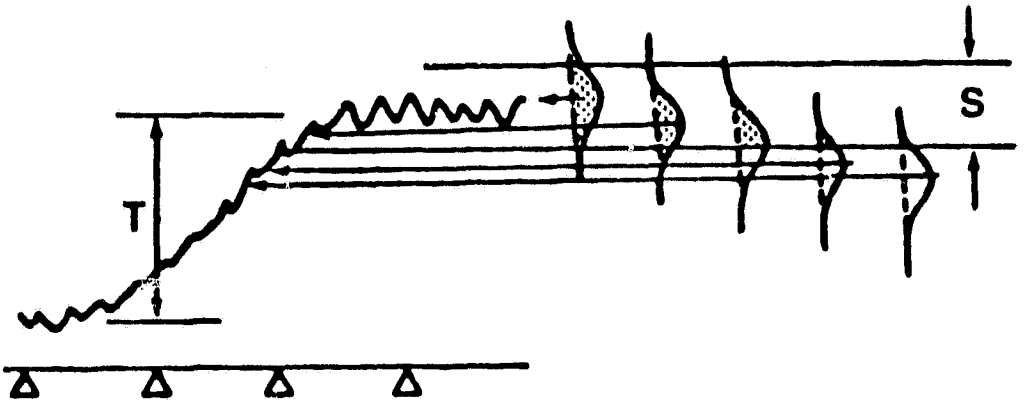

Figure S-6 The distribution of "field" pixels moves down the transition curve as the measurement point moves toward the boundary. The shaded area is the proportion which will be correctly classified.

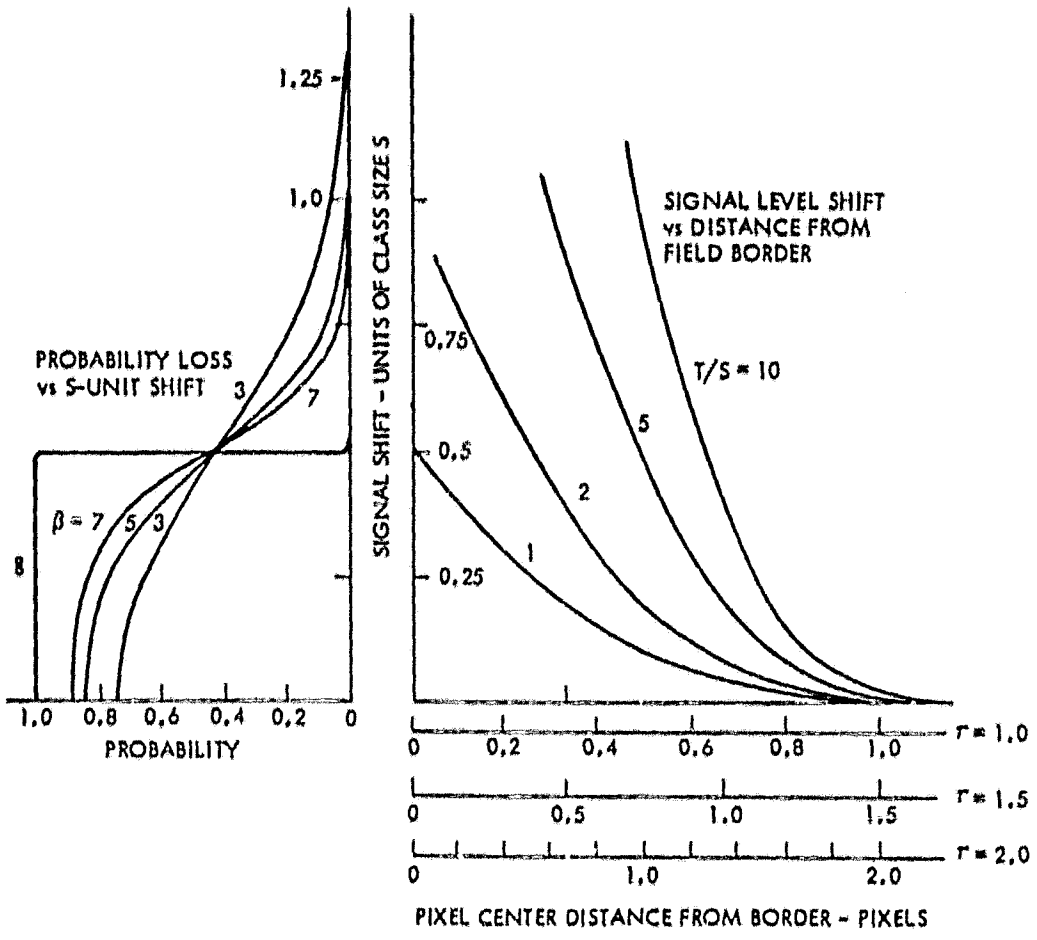

Figure S-7 Combined Curves for Translation of Pixel Distance from Border to Shift in the Brightness (Scaled in Units of Class Size, S) to Probability of Correct Classification.

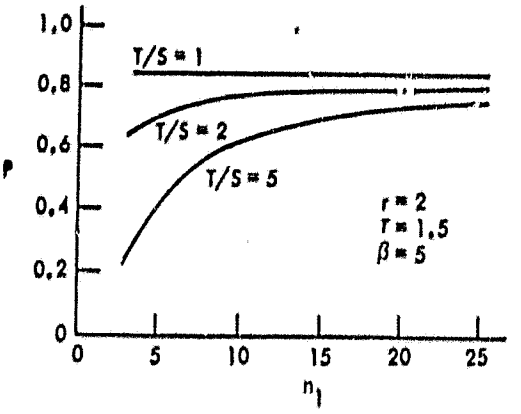

Figure S-8 Probability of Correct Classification using Global Parameters, for Perfectly Registered Pixels. One Spectral Band Only.

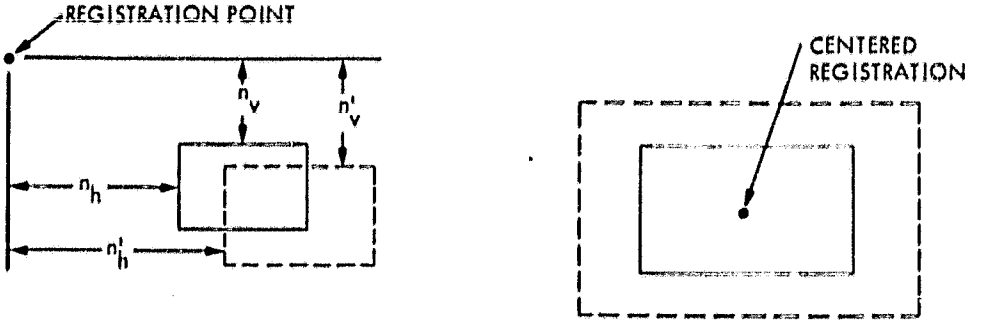

a. GENERAL CASE

b. BEST REGISTRATION CASE (NO TRANSLATION DISPLACEMENT)

Figure S-10 Construction for Estimating Misregistration Caused By Size and Aspect Errors.

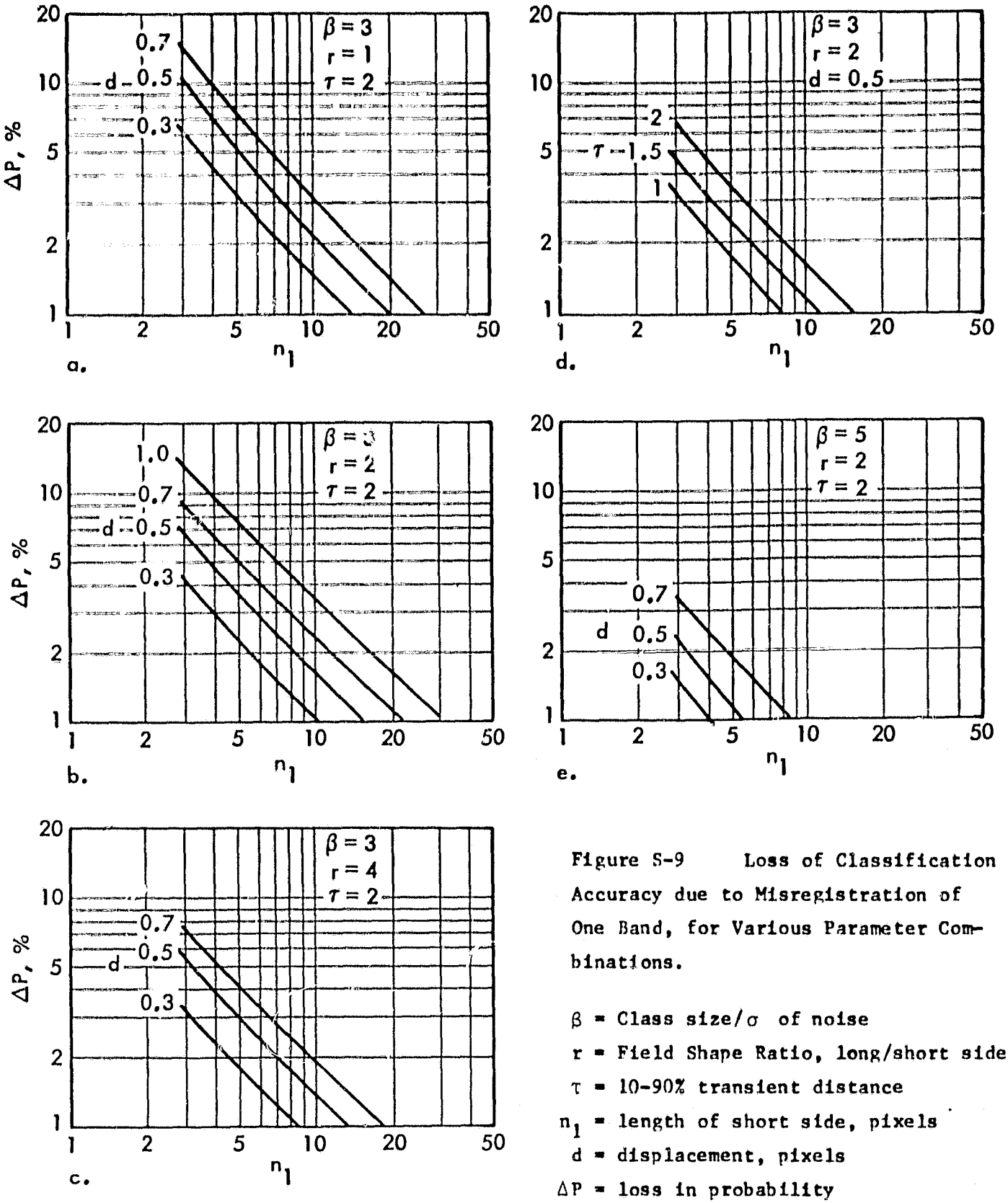

Figure S-9 Loss of Classification Accuracy due to Misregistration of One Band, for Various Parameter Combinations.

β = Class size/σ of noise

r = Field Shape Ratio, long/short sides

τ = 10-90% transient distance

n_1 = length of short side, pixels

d = displacement, pixels

ΔP = loss in probability

SECTION II

DETAILED REPORT

INTRODUCTION

Spectral analysis generally takes the form of multispectral classification in which the classification is done by comparing the sample measurement vector to the statistics of the set of known material vectors (training statistics) representing all possible classes, and by using one of several decision methods, determining which of the knowns it most nearly matches. Alternatively, pixel clusters are determined in spectral space, after which the materials forming each cluster are identified. As these have been treated extensively in the literature, the details will not be pursued here. Rather, this study will consider some perturbing effects from a generic point of view, which may allow us to judge the effects of various sources of error, and which will provide models against which empirical studies may be evaluated.

The problem pursued will be the effects of misregistration on the accuracy of multispectral classification in anwser to the question:

> What are the effects on multispectral classification accuracy of relaxing the overall scene registration accuracy from 0.3 to 0.5 pixel?

This is a problem of particular importance because of the prevalance of analyses requiring the use of data from more than one acquisition. Here, acquisition includes several spectral bands, requiring band-to-band registration, or the combination of several data sets from diverse sources, such as combining data from the multispectral scanner (MSS) and the Thematic Mapper (TM), the combination of data from both space and non-space sources, or short or long range temporal studies requiring overlay of temporally related data. These are discussed in some detail in Bryant, 1981.

Misregistration is but one of a group of parameters (noise, class separability, spatial transient response, field sizes) which must all be considered simultaneously. The thread of the argument (which is discussed in detail below) is this: any noise in the measurements (due to the scene, sensor, or the analog to digital process) causes a finite fraction of measurements to fall outside of the classification limits. For field boundaries, where the misregistration effects are felt, the misregistration causes the border in a given (set of) band(s) to be closer than expected to a given pixel, so that the mixed pixel effect causes additional pixels to fall outside of the class limits. Considerations of the transient distance involved in the difference in brightness between adjacent fields, when scaled to "per pixel", allows the estimation of the width of the border zones. The entire problem is then scaled to field sizes to allow estimation of the global effects.

This approach allows the estimation of the accuracy of multispectral classification which might be expected for field interiors, the useful number of quantization bits, and one set of criteria for an unbiased classifier.

THE BASIC MODEL

The expected effect of misclassification may be estimated by a simple first-order approach, because the differences in classification accuracy between the many classification schemes and conditions that have been tested are overshadowed by the vagaries and assumptions in the classification process, so that higher order analysis will contribute little additional understanding. Further, it is assumed that the training statistics have been correctly determined from known materials, that the decision rules have fixed the decision boundaries in multispectral space, and that the IFOV (the basic resolution of the system) is fixed. The assumption of correctness of the decision limits as set by the classifier from the training samples is crucial; it has been found (Hixson et al, 1980) that under some conditions accuracy of the training is relatively more important than selection of the classification algorithm. This analysis concerns single pixels only, without taking advantage of the possible increase in accuracy obtainable by considering the neighboring pixels or the advantages obtained by multitemporal analysis.

Consider first the probability of correct identification of a field interior pixel. Field interiors are nonuniform because of the combined effects of sensor noise, scaled to equivalent reflectivity ($NE\Delta\rho$) and inherent nonuniformities in the field itself. As these are restricted to approximately the same bandwidth, the combined effect will be the root mean square (rms) sum. In addition, quantization noise is normally combined with the other noises to form the total noise figure. The overall brightness distribution will be considered to be Gaussian - this is approximately true for field interiors, although the distribution deviates considerably toward bimodal for mixed materials at field borders.

The combined effect of these various noise sources produces a finite probability of misclassification. Precision of the classification is greatest when the known classes have tight statistics and are relatively widely separated in vector space. Addition of noise will cause the class statistics to spread, so that the separation/spread ratio decreases, and also causes uncertainty in the vector position of the unknown being classified. Keady et al (1971) have investigated this effect, and show in their Figure 12 (reproduced here as Fig. 1) an experimental decrease in classification accuracy with increasing noise.

The first-order estimate considers the total variance caused by the scene, sensor and quantization as compared to the defined class size limits, however these are determined. Similar, but relatively second-order, effects may be expected with a higher order analysis.

For simplicity, and because of the later desire to misregister one (or more) of the bands, the discussion will assume that spectral bands as sensed will be used, and that for recognition, the unknown pixel must fall between appropriate limits in every band tested. Therefore, brightness outside of a

limit in any one band is sufficient for rejection, so that we need to consider only one band at a time. The resultant first-order multispectral probability of correct classification of a given pixel is the product of the probabilities taken one band at a time.

This situation is illustrated in Figure 2, which shows the location in two-dimension decision space of four typical materials. Decision boundaries are assumed to have been determined from the training samples for the materials according to some decision rule: Figure 2a illustrates boundaries from a maximum liklihood classifier, Figure 2b illustrates manually set boundaries of a parallelepiped classifier as determined after consideration of the class spread and the tradeoff between the consequences of omission vs. comission, Figure 2c shows boundaries which closely surround the training cluster, as these might be used in ELLTAB or the Image 100. The analysis model is: Given a group of pixels having a brightness B_2 and a distribution of brightness in λ_1 space, what is the liklihood that an individual pixel will have a brightness in λ_1 which falls outside the class limits in that band? The class limits in λ_1 are determined from the classification scheme used, for the given brightness B_2, as sketched in Figure 2d. (Later, the brightness of the center of this distribution in λ_1 will be allowed to vary as misregistration causes mixed materials in this group of pixels.)

The quantized brightness level of a single pixel in a given spectral band has a finite probability of not being exactly at the grand average brightness of the field of which it is a sample (See Fig. 3). The probability of a sample being within the class limits can be derived by assuming that an ensemble of clean signals from a series of areas of the same material can be anywhere within the quantizing range with uniform probability, but individual samples are perturbed by the Gaussian noise with a distribution equal to σ. The probability distribution of the signal plus noise is found by convolving the probability distribution of the signal with that of the noise. The probability of correct class assignment (i.e., the pixel is within the class limits) is then found by integrating the probability distribution between appropriate class limits. Friedman (1965).

The probability of correct classification P thus calculated is given by:

$$P = \operatorname{erf} \frac{\beta}{\sqrt{2}} - \frac{1}{\beta}\sqrt{\frac{2}{\pi}} \left(1 - \exp(-\tfrac{1}{2}\beta^2)\right)$$

where

β = class size/σ , with class size and σ in the same units

The resulting curve is given in Fig. 4, which may be approximated for ease in further analysis in the range $1 < \beta < 7$ by

$$\beta \log P = -0.40$$

As already noted, sources of noise will be the scene itself and the sensor, both assumed to be random for this analysis. The rms sum is taken to give the total effective noise. A number of pixel measurements may be averaged together to reduce the noise before classification. This final noise figure may be compared to the width of the class to give β, from which the probability of correct classification may be estimated. This leads to the Classification Error Estimator, Fig. 5. The mathematical form of this graph is:

$$\beta = \frac{\text{class size } S}{\text{total variation}} = \frac{S}{\sqrt{\frac{\sigma_1^2 + \sigma_2^2 + \sigma_3^2}{n}}}$$

where

σ_1 = scene noise
σ_2 = sensor random noise
σ_3 = sensor quantization noise
n x n pixels are averaged together

In this figure, the upper left graph represents the rms combination of the scene noise σ with the total sensor noise $\sigma = \sqrt{\sigma_1^2 + \sigma_2^2}$, the result being scaled to equivalent 8-bit digital number (dn). The upper right graph represents the averaging of n x n pixels to reduce the effective noise. The resultant total effective noise σ_{eff} is compared with the established class size (center, right) to give β, after which the curve from Figure 4 (lower, right) converts this resultant β to the probability of correct classification, P.

Consider a scene having a field interior variation of 3% as sensed by a sensor with a total noise of 1%. The total effective noise as seen by the classifier will be

$$\sigma = \sqrt{\sigma^2_{scene} + \sigma^2_{sensor}} = 3.16\% = 8.1 \text{ dn for full scale} = 256.$$

Suppose that the class size for this classification is 25 dn. With no pixel averaging, $\beta = 3.09$, and the probability of correct classification is

$$\beta \log P = -0.4/3.09 \quad \text{giving } P = 0.742.$$

Given that 74% is not accurate enough, and that the noise and class size have been fixed by the scene and the classifier, pixel averaging of (say) 2x2 pixels will raise β to 6.18, which in turn will increase P to 86%.

The useful range of β seems to be from 3 on the low end, limited by acceptability of the classification accuracy obtained, to about 7 on the high end, limited by the scene and/or sensor noise.

Considering β in this way allows an estimation of the total noise permissable as it affects the attainable classification accuracy. If the amount of scene noise to be encountered in a given classification task can be estimated, the allowable extra noise from the sensor and quantization can be specified. This leads to an estimate of the number of bits which will be useful to be transmitted. This is developed in Appendix A. For the current discussion, noise will be considered to be the total effect from all sources.

EDGE EFFECTS

To this point, the analysis is based on pixels well inside uniform fields and well away from field boundaries. A number of experimenters have spent appreciable time discovering that classification accuracy falls off at boundaries due to what has become known as the mixed-pixel effect. We will start at that point and attempt to model the effect to allow us to quantify our expectations.

We assume as a starting point that all the spectral bands used in a classification, whether obtained from one date or a series of dates, are in perfect registration. This means that when the pixel grids from each band are aligned the data contents (field borders, roads, all features) are also aligned - note that this is more than simply having all internal distortions removed, which is all that most geometric rectifications accomplish. Misregistration will (later) be considered as the lack of alignment of the pixel grids; since the computer can only work with pixel grids, this amounts to aligning these pixel grids. This will appear to the computer as a shift in the boundaries. We assume as before that training samples are accurate and that class limits have been set from these by the classifier chosen. The classification is modeled as follows: signature shifting in any individual band will tend to cause misclassification, so that we may treat the situation one band at a time. The effects of pixel mixture in all bands may then be combined together if desired. The entire analysis simplifies to the consideration of the transient intensity shift across field boundaries as compared to the class limits and the noise components of the measurement.

For the case of one band being misaligned with respect to the rest, the resultant brightness shift due to the pixel mixture is along the spectral axis involved. The amount and direction of shift will depend on the brightness of the new material being mixed with the original, in that band. Figure 6 illustrates this for the case of a shift in physical position (misregistration) of band λ_1, considering that the true field boundaries are correctly defined in band λ_2. In the general case, the most correct position of the boundaries must first be defined, and the mislocation of boundaries in each of the spectral bands considered separately. The resultant spectral shift, no longer along any one spectral axis, may be broken into orthogonal components and the bands treated separately. For the case of internal warping such as may occur for the Thematic Mapper, rather than a simple lateral shift, some rms average of the amount of pixel shifting must be estimated, after which an analysis along the lines herein may be applied.

The first step in analyzing the spatial extent of pixel mixing across borders is to estimate the shape and extent of the transient intensity shift. If the impulse response functions or the MTFs of the various components (and, hence, the entire system) are known, a precise transient response may be calculated. For example, the specifications for the Thematic Mapper for Landsat D call for a 2% to 98% time equivalent to about 2 pixels, implying a 10-90% transient response of about 1+ pixel (Appendix B). If the true system impulse or frequency response is not known, the transient response must be estimated. For a band limited system Δx, the maximum allowed distance between samples, is given by the Nyquist criterion as $\Delta x = 1/(2f_o)$, where f_o is the spatial frequency above which there is no signal content (Figure 7). This is approximately the sampling condition of the Multispectral Scanner and of the Thematic Mapper. Most practical systems will have a roll-off in

frequency response for which an approximate transient rule of thumb is $\tau_{10-90} = 1/(3f'_o)$, where τ_{10-90} is the distance between the 10% and 90% response points and f'_o is the nominal cutoff frequency at the 70% frequency response point (Figure 7). The shape of the pass band will be approximately Gaussian, scaled to the principal determining factor, the scanning aperture size. Defining the resultant passband limit f_o as the first zero point of the sinc x defined by the scanning aperture at $x = \pi$, the 70% response point is at about $x = 1.4$. Thus $f'_o/f_o = 1.4/\pi$. Substituting $1/2\Delta x$ for f_o, and putting the resulting equation for τ gives

$$\tau_{10-90} = \frac{1}{3 f'_o} = \frac{2\pi}{3 \times 1.4} \Delta x = 1.5 \Delta x .$$

While it is realized that there are several approximations in the above, so are there in the usual basic assumption that data are Gaussian in distribution - both sets of assumptions are generally correct, and more precise mathematical formulation would not clarify the issues.

The practical result of this are:

- The "infinitely sharp" edges (narrow roads, point sources) of the real scene will be softened by the filtering effect of the scanning aperture and it is this softened transient response which is sampled.

- Adjacent samples can never have an amplitude difference more than approximately one half of the transient size.

- The proper reconstructing function for a band-limited noiseless signal with extended objects is sin x/x; if these functions are erected at each sample point with corresponding amplitudes, the softened edge will be perfectly reproduced. (But see below.) Under these conditions, the same edge shape will be produced independent of the phasing of the actual samples.

- The sin x/x reconstruction theoretically requires an infinite interpolation extent if the bandwidth is really finite, and vice versa. Thus, $\pm\infty$ of pixels is theoretically required in the reconstruction. Since it is incongruous to believe that pixels more than a certain distance (say, ±4 pixels) have affected the sample at a given location, interpolation functions utilizing only a finite number of supports must be sought. Candidates for this are cubic splines, such as the TRW spline, B-splines (probably also cubic), splines under tension, and the Bendix restoration. The argument is that if there is no memory after a certain distance (the autocorrelation distance), pixels and, therefore, the interpolation basis functions beyond that range will have zero benefits, and for practical systems, will only add extra noise (Appendix C).

- Substitution of these various interpolation functions should have minor effect on the rise distance estimated here.

The transient situation across a border is sketched in Fig. 8a. We are concerned here with the decrease in probability that a given pixel will have a value within the class limits as that pixel moves toward the boundary, as shown in Figure 8b. This effect by itself will cause a bias in any classifier due to loss of border pixels. This loss is usually estimated by adding back into the area equivalent fractional pixels estimated from the amount of adjacent material mixing as determined from the amount of pixel brightness shift. Alternately, the loss may be avoided by proper choice of the class limits; the conditions for such an unbiased classifier are developed in Appendix D.

The analysis, therefore, only needs to determine the area under the normal curve (assuming the noise is Gaussian) between the limits as determined by the classification class size and the offset from the "field interior value" caused by the mixture. Practical values of β (ratio of classification limit size to rms noise) will be bracketed by unacceptable classification accuracy on the low end ($\beta \approx 3$) and unattainable signal to noise on the high end ($\beta \approx 7$ to 10).

First, consider that the class limits are accurately set so that the distribution of the field interior pixels is at the center of the class. Then allow the distribution center to shift (because of the mixture at a boundary) with respect to the class limits. The important scaling involved is the amount of signal shift caused by the transient total shift T, as related to the desired class size S, for a given β. The set of curves of Figure 9a reflect the portion of the area under the noise component Gaussian distribution as that distribution is intercepted by the class limits when the brightness center moves away from the class center as the pixel approaches the field boundary. These curves are optimistic in that they assume that a real field average will always be centered within the class limits. This condition would only be attained with perfectly representative training samples, no atmospheric or bidirectional reflectance effects, all samples at the same phenologic stage, etc. As these conditions normally cannot be expected simultaneously, the unknowns to be classified will likely be more uniformly distributed, so that the probability situation described for the classification accuracy derivation is more realistic. When the limiting field center (zero offset) values are modified to agree with the curve of Figure 4, the basic curves of the probability of correct identification as a function of the shift of intensity values result (Figure 9-b).

The next question to answer is how rapidly (in distance) does the shift take place? The transient rise distance estimated for the Thematic Mapper (Appendix B) has very close to a Gaussian shape and a $\tau_{10-90} = 1.5$ pixel. The amount of brightness shift is the difference between the brightness of the field under consideration and the adjacent field which is causing the shift. The important intensity relation is the magnitude of this shift, T, as related to the size S of the class being tested by the ratio T/S. These curves, for various T/S, may be combined with those of Figure 9-b to give Figure 10. From this may be estimated the loss in probability in classification of pixels near borders.

The curves as given are optimistic in that they are based on the best-case transient rise distance. Any deteriorating effect, such as atmospheric scatter or turbulance, which injects light into the image of a given field from adjacent image areas, will raise the effective transient distance as well as cause a veiling haze (the path brightness). A realistic estimate may consider the transient distance to be perhaps 1.5 to 2 pixels; 1.5 will be used in the remainder of this report.

BIAS IN FIELD SIZE ESTIMATION

It can be appreciated from Figure 8 that several things are happening simultaneously: If the lower limit of field B and the upper limit of field A have a gap between, pixels "lost" by field B will not be picked up by field A, and will be considered unknowns and not be counted in either field. The lost pixels will be some interior pixels, due to insufficient β, and a large number of near-border pixels, resulting in apparent field size loss. Only if the lower limit of field B and the upper limit of field A are coincident will pixels lost from one field be picked up by the other, and vice versa, to give complete account of all pixels. For the field size estimator to be unbiased, the loss-and-pickup in both directions must cancel; that is, on the average the true border must be located.

The various estimations of the transients across borders predict negligible phase shift; that is, the 50% response point occurs at the true border. This implies directly that the true border can be located from the data if the decision brightness is midway between the brightnesses on either side of the border. However, even if phase shift lag causes border displacement, the 50% response point still represents the unbiased condition. If the lag is widely different in the various bands, relative (between band) border shifting will occur. For this reason, the transient response of the various bands should be matched as closely as possible. It is likely that this 50% setting of the decision brightness will not be the same as would be calculated by a classifier; indeed, it cannot, as the field edge decision brightness will vary even for a given field as the adjacent fields vary in composition. This leads directly to the required algorithm for field size estimation: First divide the scene into blobs, each of which is sufficiently uniform, and with closed boundaries. Then for each blob (field) determine the average brightness for all the interior pixels which are safely away from the border. For each segment of the border, the correct field edge decision level is midway (in σ's) between the average brightness of the two fields on either side. Then, if desired, the field interiors may be reclassified using the classification limits as determined from the training samples.

The total effect will depend on the ratio of the number of border pixels to the number of field-interior pixels, and hence is a function of the field shape and size. This is developed in some detail in Appendix D. The important conclusions which can be drawn are:

- For accurate field size estimation, the decision brightness must be halfway between the brightnesses of the fields on either side of a given boundary. This means that classifiers set for material identification will in general produce errors in field size.
- Correct Nyquist sample spacing is about equal to 2/3 of the 10%-90% transient distance. But relaxation to about equal this distance causes little problem.
- It is important to keep the transient distance small, to get as many pixels into a given ground distance as possible. Field area errors become large at $n_1 = 5$ or less. The transient distance must also be matched between spectral bands.
- It is most critical to keep the decision limit midway between the adjacent-field brightnesses for small fields. But this is increasingly hard to estimate for small fields because of the fewer interior pixels.

- At the resolution expected for the Thematic Mapper, the atmospheric point spread function may become more dominant than the Thematic Mapper point spread function. If this is determined to be true, the registration requirements may be relaxed.
- The total noise figure (compared to the class size in a given determination) controls β, and in turn controls the maximum attainable classification accuracy. However, for practical range of $3 < \beta < 7$, increasing β has only a moderate effect.
- Because of this, if small fields are most important, the reflected energy might more profitably be divided into smaller pixels, even at the expense of $NE\Delta\rho$. As this will cause an increase in data rate, optimum coding should be investigated. The possible noise introduced in reconstructing the data will cause some further decrease in the overall effective $NE\Delta\rho$ and so decreases β. But since there is smaller sensitivity to β than to $1/n_1$, there should be a net gain in utility.
- Geometric rectification and registration procedures must not only remove the internal distortions but must also produce pixels on a defined (preferably ground-referenced) grid. Current procedures do not do this. Without this reference grid, users will have to reinterpolate before multi-temporal data can be compared.

EFFECTS OF MISREGISTRATION

In preparation for estimation of the misregistration effects, an analysis will first be made of the expectations of registered data and the sensitivity to the various parameters estimated. Pixels will be grouped into four zones: 1) Interior - those with centers 2 or more pixels inside borders; 2) Inner border - pixels with centers 1-1/2 pixels inside borders; 3) Outer border - pixels with centers 1/2 pixel inside borders; 4) Exterior border - pixels outside the borders, with centers 1/2 pixel outside. This is illustrated in Figure 12. Estimates of classification accuracy for each zone will be obtained from Figure 10. The total estimate of calssification accuracy will be the sum of pixels in each zone multiplied by the corresponding zone accuracy estimate. Later, the field will be misregistered, changes in the number of pixels in each zone calculated, and the probabilities again summed.

As before, define

n_1 = number of pixels in field short side
n_2 = number of pixels in field long side
$r = n_2/n_1$, the field shape ratio

The numbers of pixels is:

n_i	; Interior	:	$(n_1-4)(n_2-4) = (rn_1-4)(n_1-4) = rn_1^2 - 4(r+1)n_1 + 16$ Note that this = 0 for $n_1 \leq 4$.	
n_{ib}	; Inner Border	:	$2(n_1-2) + 2(n_2-4) = 2(r+1)n_1 - 12$	$(n_1 \geq 4)$
n_{ob}	; Outer Border	:	$2(n_1) + 2(n_2-2) = 2(r+1)n_1 - 4$	
n_{xb}	; Exterior Border	:	$2(r+1)n_1 + 4$	
	Total Area	:	rn_1^2	

Note that r may vary over a significant range, and that the later misregistration analysis applies to a pair of field images having precisely the same r value and precisely the same size, but displaced one from the other without rotation.
The total probability of correct classification is given by

$$P = \frac{1}{rn_1^2} \left(p_i n_i + p_{ib} i_{ib} + p_{ob} i_{ob} + p_{xb} i_{xb} \right)$$

The details are worked out in Appendix E.

From the derivations in Appendix E, the following global values may be selected for the parameters:

$r = 2$
$T/S = 1$ to 5
$\tau = 1.5$ pixels
$\beta = 5$

The resultant probability of correct classification for the global set of parameters is given in Figure 11 (derived from the general curves of Figure 10).

After the parameters r, T/S, τ , and β are selected, the resultant probabilities may be substituted for the brightnesses in the various zones to produce a "probability image" aligned with the desired output pixel grid. The probability assigned to a pixel at a given location represents the probability that that pixel will have a brightness falling within the classification limit determined by the classifier, for the given spectral band. The total resultant per pixel probability image for the effect of q acquisitions is obtained by superposing the q probability images and multiplying together the set of q probabilities for each pixel point. An acquisition is defined to be each band or data set used simultaneously. Using these values, the global estimate of the probability of correct classification for one acquisition with no misregistration is given in Figure 13 for three values of T/S. The predominant effect is the pixel mixture (the effect of T/S). This is worst for small fields (n_1 small) because of the larger percentage of border pixels for these fields. Note that for T/S = 1 (the same as $\delta = 1/2$ of Appendix D), no probability loss occurs, even with small fields. Unfortunately, this desirable condition cannot be systematically obtained.

MISREGISTRATION OF CONGRUENT FIELDS

Figures E-5 and E-6, and the accompanying discussion in Appendix E describe the misregistration situation. The essence of the result is that some area is lost from the external border, causing a further classification decrease. The basic character of this misregistration loss term is $1/n_1$, so that it will have a slope approximately equal to -1 on a log-log plot vs n_1. The precise results depend critically on the values estimated for the p_{xb} from Figure 10. The values chosen leading to Figure 14 are given in Table E-4.

Note first that for large T/S (i.e., 2 or more) the edge effects are so great that the base probability is drastically affected (Figure 13), and that the external border pixels have zero probability of being within the class limits (Table E-4). For this reason, there is no misregistration effect for large T/S, and Figure 14 is plotted for only T/S = 1.

Comparison of Figure 14-a,-b, and -c shows the effect of changes in r, with the square fields showing the most misregistration loss. As before, r=2 is believed to be representative.

Comparison of Figure 14-b and -e shows the effect of increase in β. The decrease in misregistration loss with higher β is evident. However, these losses in general are small to begin with, and the previous discussion calling for sacrifice of β to gain smaller IFOV (more pixels n_1 into a given field) would seem to override.

Figure 14-d indicates the effect of transient rise distance. Various models of the expected distance yield $1 < \tau < 2$, and this range is included in the figure. Increase in τ decreases the basic accuracy of edge pixels (Figure 11) and also increases the misregistration losses (Figure 14-d).

The curves of Figure 14 may be (even further) approximated by $\Delta P \% = K \frac{d}{n_1}$ where K is given by:

β \ τ	1.0	1.5	2
3	18	23	35
5	6	8	12

and T/S = 1, r = 2.

COMPARISON TO OTHER STUDIES

1. Proportion of Mixed Pixels

The mixed pixel problem has long been recognized. Nalepka and Hyde (1972) estimated the percentages of mixed pixels in agricultural scenes to be between 20 to 40 percent, depending on the field sizes. Pitts and Badhwar (1980) obtain about the same percentage for field in the United States Great Plains. Chittineni (1981), in estimating the proportion of components within each mixed pixel, also finds a large proportion of mixed pixels in a scene.

2. Scene Segmentation and Blobbing

In addition to the blobbing referenced in Appendix D, Bryant (1979) and Kettig and Landgrebe (1976) have attempted to segment scenes into "pure" pixels and mixed pixels.

3. Size and Shape Parameters Verification (n_1, r)

Figure 15 provides the scaling needed to put the prior analysis into the real world, relating the field width n_1 to area for the assumed shape ratio r = 2, for Thematic Mapper pixels.

It has been shown that r = 2 is a good model for a range of ratios. That this also represents the real world is shown in the table below, using

data from Podwysocki's report "An Estimate of Field Size Distributions for Selected Sites in the Major Grain Producing Countries", GSFC X-923-76-93.

Location	Shape Ratio	50%-of-fields width-Pixels	50%-of-area width-Pixels
Kansas	1.71	8	9.5
Iowa	1.78	9	10.5
Saskatchewan	1.98	11	15
USSR 1	1.39	25	31
USSR 2	1.53	20	30
PRC 1	1.48	7	9.5
PRC 2	1.37	8	9.5
France	1.44	5	6
India	3.09	2	5
Average except India	1.58	11.6	15.1

Given the relative insensitivity of the results to the ratio r, the assumed r = 2 would seem to be representative.

Also from Podwysocki's report (Figures 16 and 17) the area and field width distributions are given in the table. It can be seen that (except for the many small narrow fields in India) the 50%-of-the-fields width is about 12 pixels and the 50%-of-the-area width is about 15 pixels. However, to accurately estimate the total area, many more of the smaller fields must be classified. Taking the 10%-of-the-area point as the limit, the field width is about 8 pixels. Thus the field size range of primary interest is from about 5 to 30 pixels. Again, India is low, with a 10% point at about 2 pixels.

The Hughes"Thematic Mapper User Sensitivity Study Report" (July 1980) considers only one field size and shape, 14x14 pixels, in the simulation. Given the field size distributions from Podwysocki's report, this 14x14 size does not seem to include the more critical small sizes. For this reason, the combined bulk and boundary classification losses quoted are optimistically low.

4. Adjacent Field Transient Brightness Shift Verification (T,S)

There is no data for the amount of transient edge shift to be expected. An intuitive feel is that during the growing season all fields will be vegetated, either with the crop of interest or an alternate crop. To the extent that "green is green", and except during the period when different crops have widely different phenologic stages, the signatures will be similar. Therefore, the decision limits must be close to the field interior averages, and the β will be low. Also, in this study no account has been taken of field edge artifacts: hedgerows, roads, ditches and the like. For small fields, these may introduce appreciable further error, as they will form an appreciable part of the mixed pixels.

The Hughes report lists the set of 8 classes used in the analysis. However, no data is given for the class brightnesses nor the variance used in the simulation. Thus, there is no way to estimate the β which was effective during the analysis, nor the adjacent field transient brightness change T, nor the effective class limits S. However, the statement is

made "...the classes used for this simulation are inherently more separable than those used by GE." This would imply the use of a high β. This is verified by the unusually large within-field accuracy obtained - in the >95% range, requiring a β of 10 or more.

The Hughes report correctly states "Depending on the threshold values used ... results could be better or worse than those obtained by performing multiple class classifications. Finally, the reader is cautioned to use the classification accuracy only in a relative sense to compare effects of the TM parameters. The absolute classification accuracy losses will be dependent upon the particular scene and the statistical separation of the classes being investigated." Although this is true, simulations should approximate reality to be useful. The GE study, which concentrates on agricultural subscenes, is more representive of the tasks (e.g. LACIE, AGRISTARS) for which classification accuracy is most critical, and the larger effects of the TM parameters and misregistration are probably more realistic.

5. Adjacent Field Transient Distance (τ)

The necessity of maintaining a low transient distance τ is illustrated by Figures 11 and 14-d. This distance is the result of the convolution of the optical blur, diffraction, detector size, and filter. The Hughes report shows that "...convolution with the relatively large square TM detector and the electronics modulation transfer function (MTF) virtually eliminates any differences created by various shapes of blur... The largest degradation in image quality is caused by slow rise times or mixtures of filters." All of the filters simulated show a τ_{10-90} of about 1.3+ pixels, except the undershoot filter, which had a τ_{10-90} of 2.4 pixels (Hughes Figure 5). The insensitivity to the exact filter shape (except the undershoot) justifies the use of a Gaussian rise as surrogate. The assumed global value assumed here of $\tau_{10-90} = 1.5$ seems realistic, although perhaps a bit optimistic. The potential further blurring by the atmosphere, which will affect the total system performance, is neglected as it is not a hardware parameter.

The large transient distance, large delay (about .8 pixels more than the protoflight or ideal filters), and slow settling time of the undershoot filter reinforce the Hughes statement as to the need to match filters, and, in particular, to avoid the undershoot case.

It is shown in this study that edge pixels affected by adjacent fields are those within 2 pixels of the boundaries. The Hughes study considers boundary pixels to be those within 3 pixels of a boundary. Although the difference seems small, this is an appreciable part of a small field, and includes one row of pixels which is not affected except at very large τ. Therefore, the loss in accuracy of boundary pixels is underestimated in the Hughes report.

6. Type Of Misregistration

The misregistration errors can be classed as displacement or distortion, depending on whether the area of interest is mislocated or distorted.

Some typical causes are:

Displacement - the area of interest is mislocated

Scan velocity changes
Alignment Errors
Warm to Cold Focal Plane
Platform Vibration
General mapping projection on round earth (Multitemporal problem)

Distortion - the area of interest is distorted

Scan Line Corrector
Nearest Neighbor Interpolation
Altitude Relief Displacement (Multitemporal Problem)

Total misregistration effects, whether caused by displacement or distortion, will be considered (without mathematical justification) to be the rms of the various individual causes, and treated as a displacement. (a brief discussion of this is given in Appendix E).

Band to band displacement as caused by scan velocity changes from nominal may be estimated from the focal plane layout, Figure 18. Considering Band 4 as a reference, the distance in pixels to the other high resolution bands is:

Band	5	7	3	2	1
Distance	71	45	25	50	75

The rms of these distances is 125 pixels. Considering that the scan velocity may be 0.5% away from nominal, the resultant rms displacement of the bands is 1/2%x125 = 0.62 pixels. If the scan velocity error cannot be maintained to considerably below this value, band to band registration will be required. If the velocity can be measured or modeled (even if not controlled), this registration may be done by calculation; if not, band to band correlation will be required over the face of each scene. The criticalness of at least measuring the velocity is evident.

The various alignment errors presumably can be calibrated once and applied to the total image (although perhaps on a band to band basis).

Platform vibration will add an additional apparent scan velocity component when the IFOV is projected to the ground. Considering that the IFOV scans at a rate of about 0.13 rad/30 msec = 4.5 rad/sec on the ground, holding the spacecraft vibrations to (say) 0.1% effective change in scan velocity to minimize the band to band displacement requires holding the vibration velocity peaks to about 5 mrad/sec. Again, the utility of measuring or modeling this velocity is evident.

Displacement errors of a different type affect the ability to easily do multitemporal overlays. These are the large area low spatial frequency warping distortions, caused by the projection to the earth (altitude, attitude), scan velocity integrated effects, and spacecraft vibration. These can be modeled and a first order blind correction made, if sufficiently precise measurements are made. The GE report "Geometric Correction Matrices for Thematic Mapper", dated 4/22/80 covers this in detail. Of interest to the

eventual data user is the grid to which the data are transformed: "Output scene coordinates are an XY system with origin at the scene center. Direction of Landsat-D motion is in the direction of the -Y axis." Because of this, each scene will be on a different grid, and even nominal repeat scenes will not have common grids. Assuming that all of the warping has been correctly removed, for many uses users will still have to resample to common grids, dealing with translation, rotation, scaling, and recasting to the desired working map projection.

Relatively few, if any, users will be in a position to perform all of the corrections outlined in the GE report. Thus, if the images are properly prepared and archived with complete enough annotation that data from a given ground location can be expeditiously extracted, there should be relatively little traffic for the raw data. Because of the independent grids, of top importance is that the system-induced internal warping be removed from images supplied to users to minimize the further detailed correlations which the users must perform for registration and to allow the production of undistorted film images.

Instrument-associated distortion removal is discussed in the GE report, but no feel for the adequacy is available. The deleterious effects of nearest neighbor interpolation are discussed in Appendix C of this report. A remaining prime distortion effect is that caused by relief displacement as the altitude of the ground at various places in the scene changes. Although not an instrument problem, it will be a system problem. The construction is given in Appendix F and the net result in Figure 19. The essence of the argument is that, without relief displacement correction, map accuracy at 1:24000 (approximately 0.4 pixel) data location and image registration to fractional pixel cannot be met in areas of high relief. Thus, for precision work, many users must perform precision correlation and interpolation over the entire face of an image, and/or use pixel-scale altitude data in an open ended correction.

DATA UTILITY

This report is an attempt to model the potential misregistration effects on multispectral classification accuracy. It may allow the comparison of the various tests and simulations, and points out the variables which must be reported for those simulations to allow their validation. Unfortunately, most simulations are not accompanied with sufficient data to provide understanding of the precise conditions under which the (e.g.) classifier operated. Because of this, it is difficult to judge the degree to which the simulation is a good surrogate for the real world, and difficult to compare the simulations.

For many purposes, multispectral classification is not the required data analysis procedure. Although many of the concepts herein may be applied to other analysis procedures , other factors not considered may overshadow conclusions reached by this modeling. For example, precision location of boundaries in the image for mapping purposes will invoke a different set of criteria. Image feature interpretation, especially of features in which the brightness does not have abrupt boundaries, will also be different.

Finally, the analysis does not answer the bottom line question even if multispectral classification is the required procedure: Given a certain loss in accuracy, how does that damage the ability to use the data analysis results? Or: Given that the system produces data to a certain registration accuracy, how much additional work, by how many users, will be required to bring the data to sufficiently good registration for (each of) their needs? These evaluations will be discipline dependent, and must be sought separately.

REFERENCES

2-1. Bryant, J. (1979) On the Clustering of Multidimensional Pictorial Data, Pattern Recognition, Vol. 11, #2, pp. 115-125

2-2. Bryant, N.A. (1981), Issues Relating to Registration of Landsat MSS and TM Systems, Jet Propulsion Laboratory, in preparation.

2-3. Chittineni, C.B. (1981) Estimation of Proportions in Mixed Pixels through their Region Characterization, (Personal Communication)

2-4. Friedman, H.D., (1965), On the Expected Error in the Probability of Misclassification, Proc IEEE, Vol. 53, p. 658.

2-5. General Electric (1979), Thematic Mapper Performance Parameters as Related to User Considerations, for NAS5-23412 Amend 165, June 15, 1979.

2-6. General Electric (1980), Geometric Correction Matrices for Thematic Mapper, Program Information Release, P. Jasper to E. Beyer, April 22, 1980.

2-7. Hixson, M., Scholz, D., Fuhs, N., Akiyama, T., Evaluation of Several Schemes for Classification of Remotely Sensed Data, Photogrammetric Engineering and Remote Sensing, Vol 46 #12, Dec. 1980, pp 1547-1553.

2-8. Hughes (1980), Thematic Mapper User Sensitivity Study Report, Contract #NAS5-25588, for Goddard Space Flight Center, July 1980

2-9. Kettig, R.L. and Landgreke, D.A., (1976) Classification of Multispectral Image Data by contraction and classification of Homogeneous Objects, IEEE Trans. Geoscience Electronics, Vol. GE-24, pp. 19-26.

2-10. Nalepka, R.F. and Hyde, P.D., (1972) Classifying Unresolved Objects from Simulated Space Data, Proce.8th Symposium on Remote Sensing of Environment, Environmental Research Institute of Michigan, Ann Arbor, Michigan, pp. 935-949.

2-11. Pitts, D.E. and Badhwar G., Field Size, Length, and Width Distributions based on Ground Truth Data, Remote Sensing of Environment, Vol 10, pp. 201-213.

2-12. Podwysocki, M.H. (1976a) An Estimate of Field Size Distributions for Selected Sites in the Major Grain Producing Countries, Document #X-923-76-93, Goddard Space Flight Center, April 1976.

2-13. Podwysocki, M.H. (1976b) Analysis of Field Size Distributions, Lacie Test Sites 5029, 5033, and 5039, Anhwei Province, People's Republic of China, Document #X-923-76-145, Goddard Space Flight Center, June 1976.

2-14. Ready, P.J.,Wintz, P.A., Whitsitt, S.J., Landgrebe, D.A., Effects of Compression and Random Noise on Multispectral Data, Proc 7th Symposium on Remote Sensing of the Environment, Univ. Michigan, 1971, pp 1321-1343.

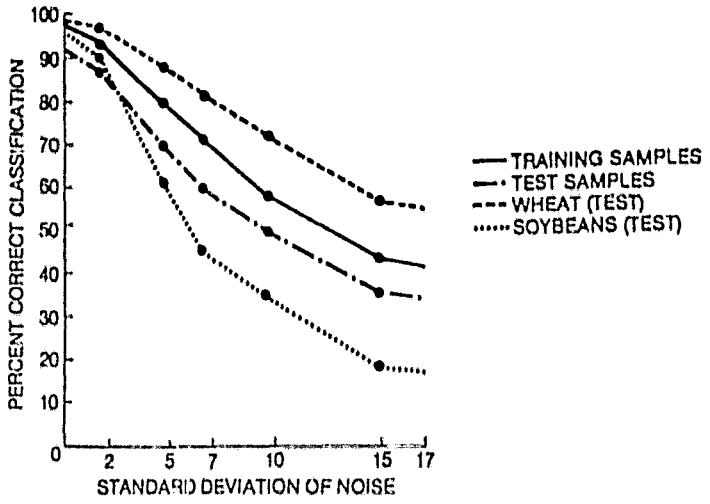

Figure 1. Effect of random noise on the accuracy of multi-spectral classification. (From Ready 1971)

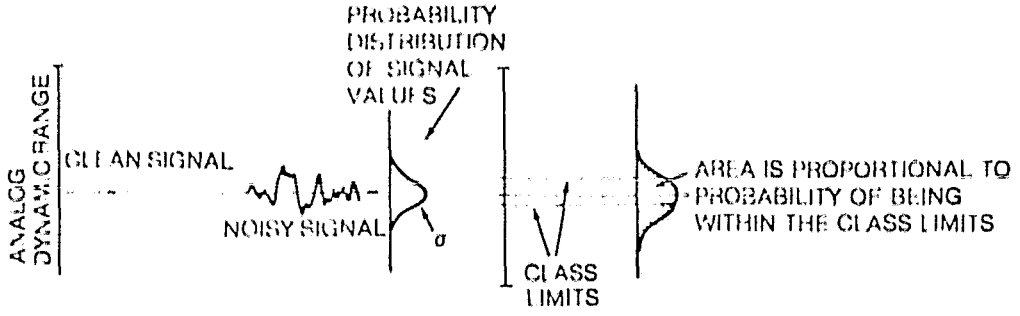

Figure 3. Effect of noise on the probability of correct multi-spectral classification.

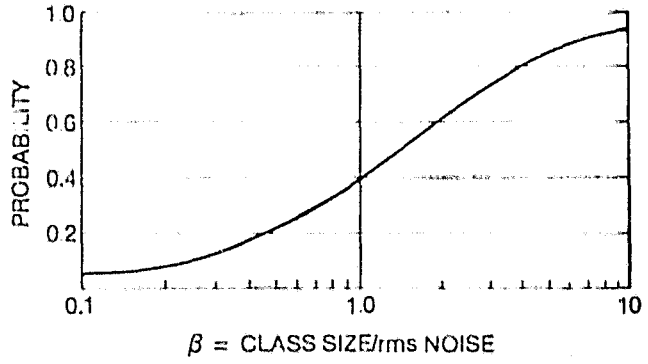

Figure 4 Given a signal uniformly probable over the dynamic range. Gaussian noise of value=σ. The curves show probability of correctly recognizing a class corresponding to the noise free signal as a function of the ratio β = class size / σ .

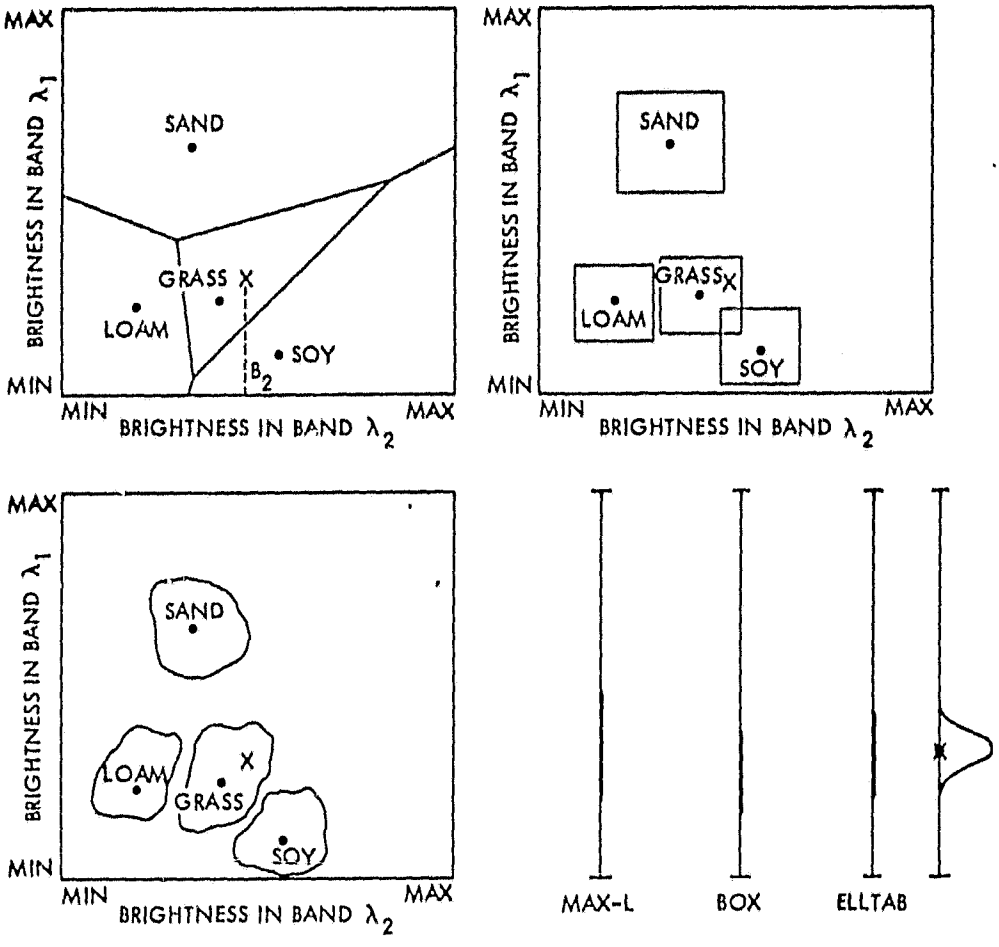

Figure 2. Location of typical materials in 2-dimensional decision space, with decision boundaries as determined by a) (Upper Left) Maximum-likelihood; b) (Upper Right) Parallel piped Box; c) (Lower Left) Defined Clusters, as in ELLTAB or Image 100. For a given brightness B_2 in spectral band λ_2, the class extent for "Grass" in band λ_1 is shown for each classifier in Figure 2d (Lower Right), together with the location in band λ_1 of the distribution of pixels of a group located at position "x".

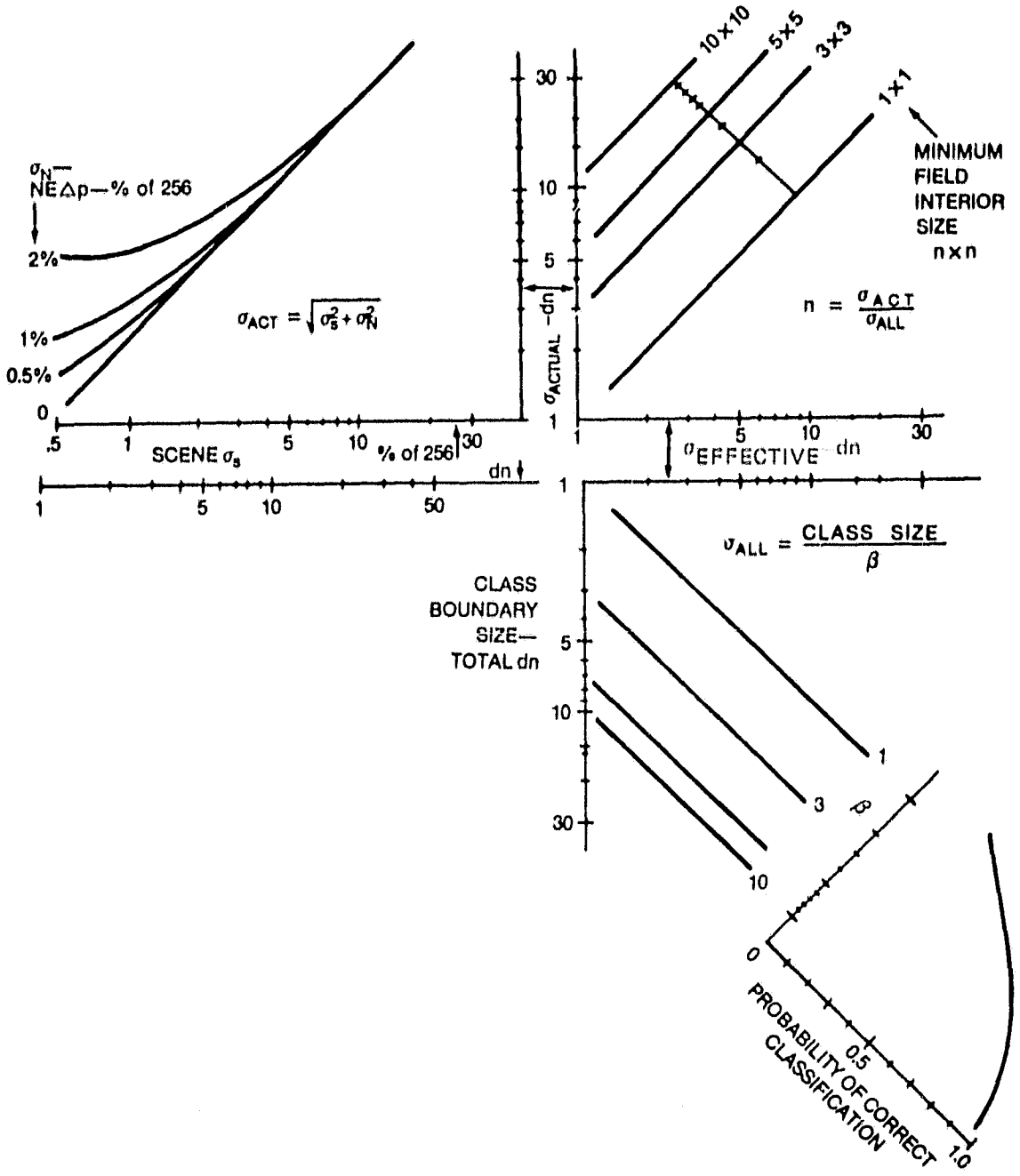

Figure 5. Classification Error Estimator

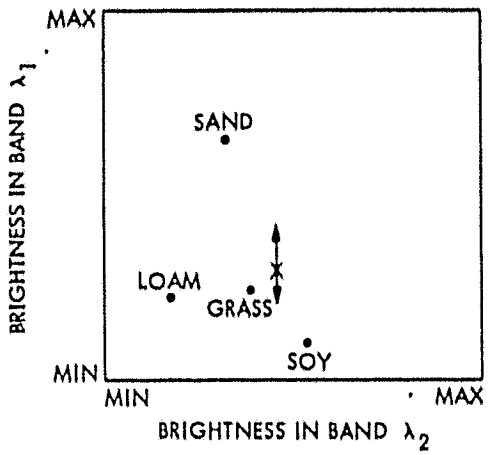

Figure 6a (Left) Misregistration of band λ_1 causes the brightness in this band to vary. For one band misregistration (in this case, λ_1) the intensity variation will be aligned with the spectral axis in decision space.

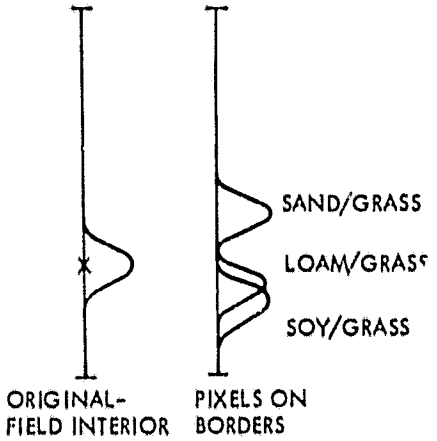

Figure 6b (Right) The amount and direction of spectral shift depends on the mixture, determined by the adjacent material.

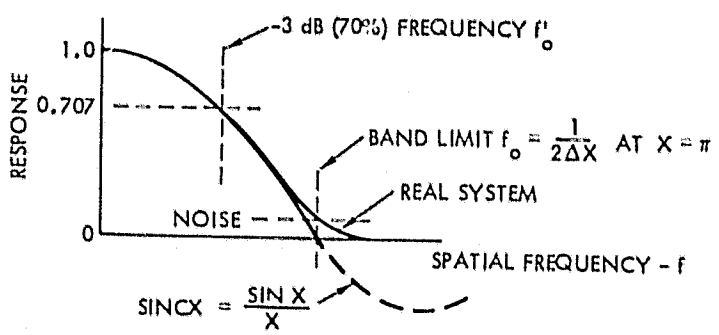

Figure 7 Construction for Relating Spatial Frequency to Transient Distance

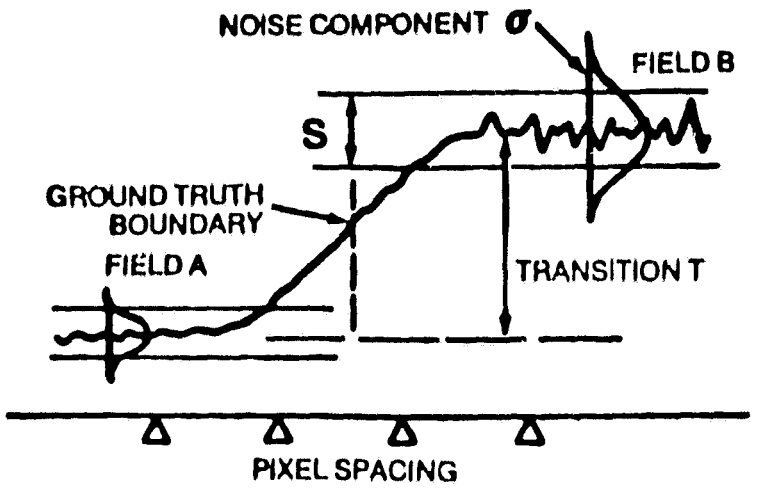

Figure 8a Cross section of brightness trace across a boundary between two fields, showing the distance required for the brightness transition.

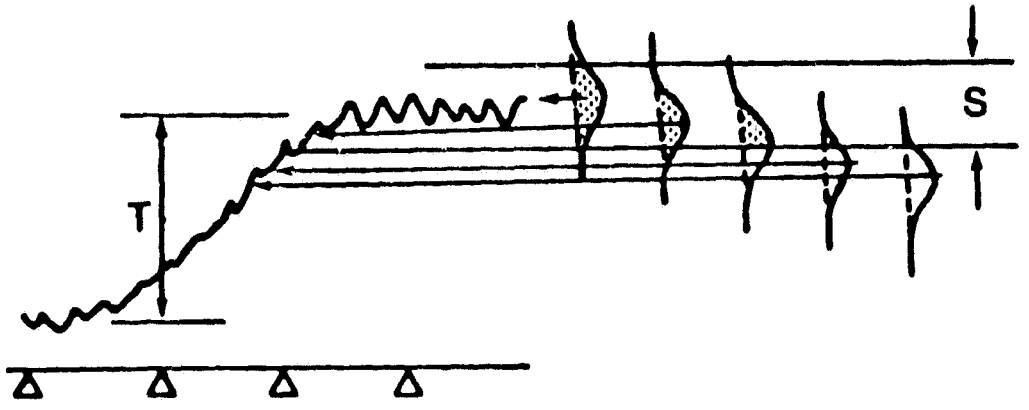

Figure 8b The distribution of "field" pixels moves down the transition curve as the measurement point moves toward the boundary. The shaded area is the proportion which will be correctly classified.

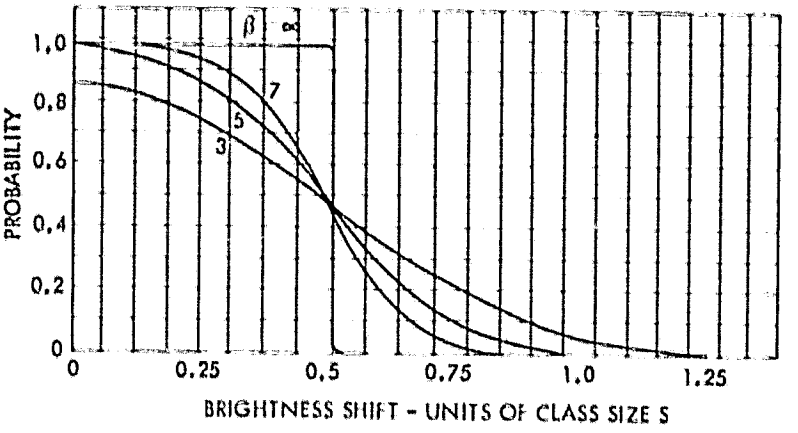

Figure 9a Loss in Probability of Correct Classification as the Brightness of a Group of Pixels changes - curves for Precise Centering of the Initial Group within the Class Limits

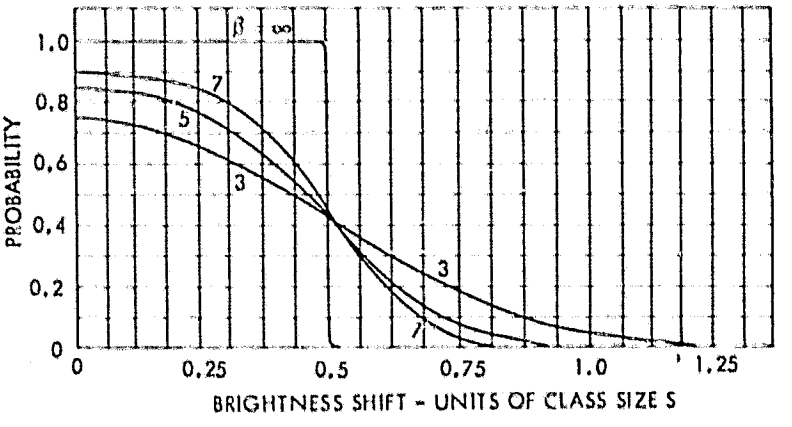

Figure 9b **Loss in Probability of Correct Classification as the Brightness of a Group of Pixels Changes - corrected Curves**

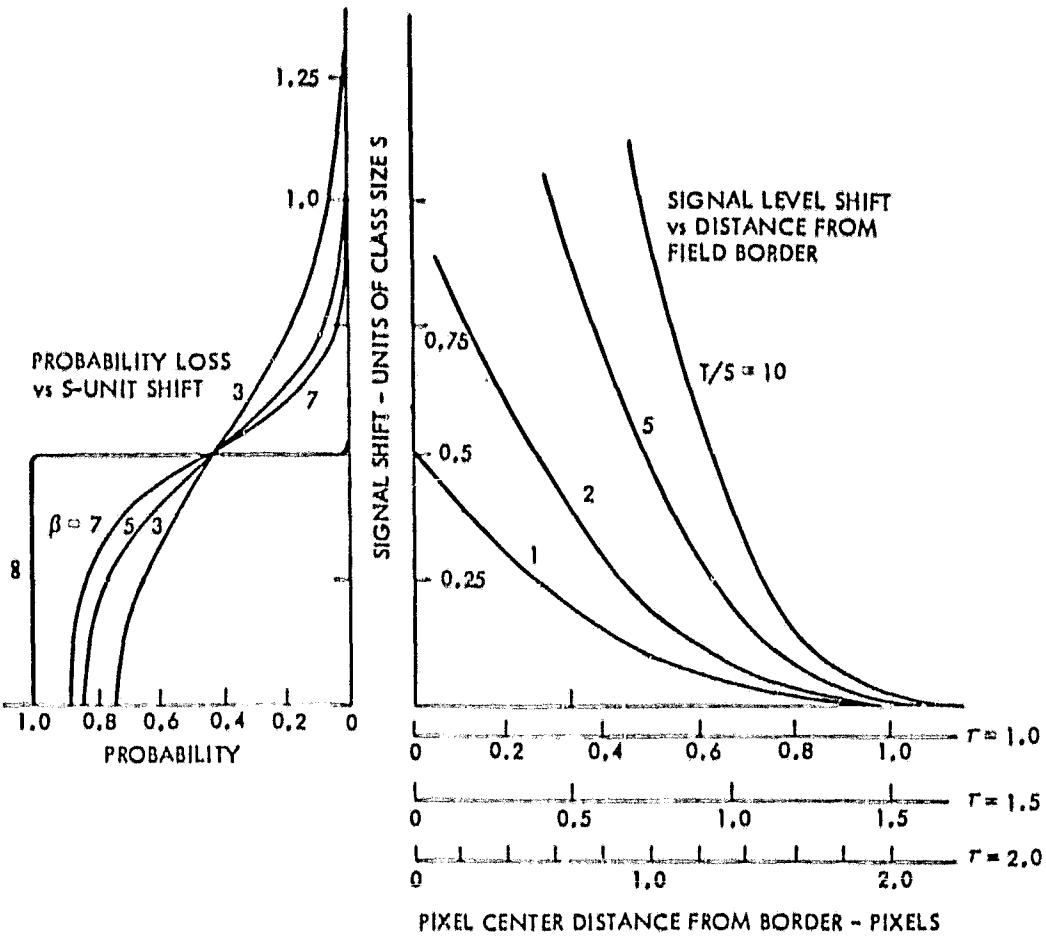

Figure 10 Combined Curves for Translation of Pixel Distance from Border to Shift in the Brightness (Scaled in Units of Class Size, S) to Probability of Correct Classification.

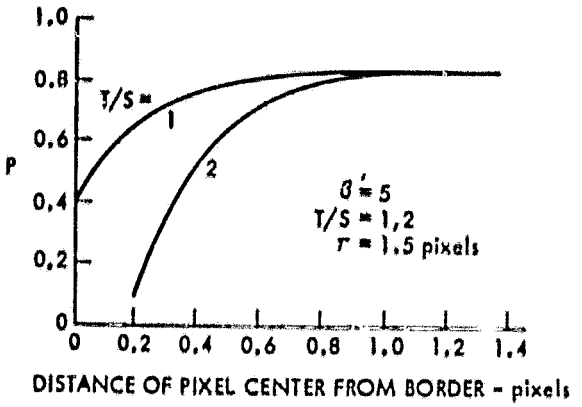

Figure 11 Probability of Correct Classification of Individual Pixels as a Function of the Distance of the Pixel Center from the Field Border

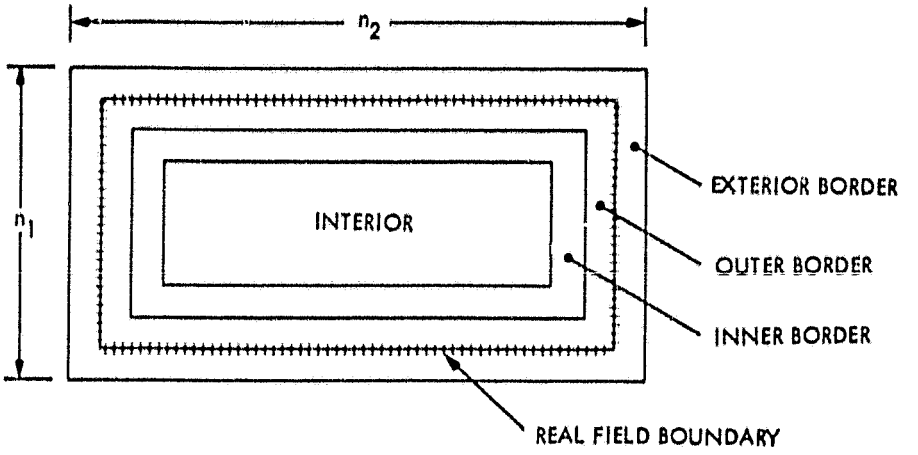

Figure 12 Construction for Estimating Total Effect of Border Pixels, with Perfect Registration

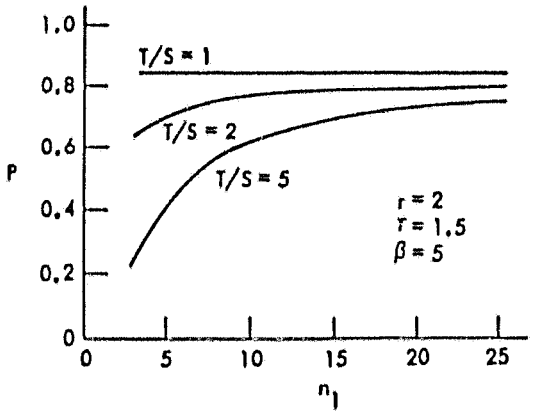

Figure 13 Probability of Correct Classification using Global Parameters, for Perfectly Registered Pixels. One Spectral Band Only.

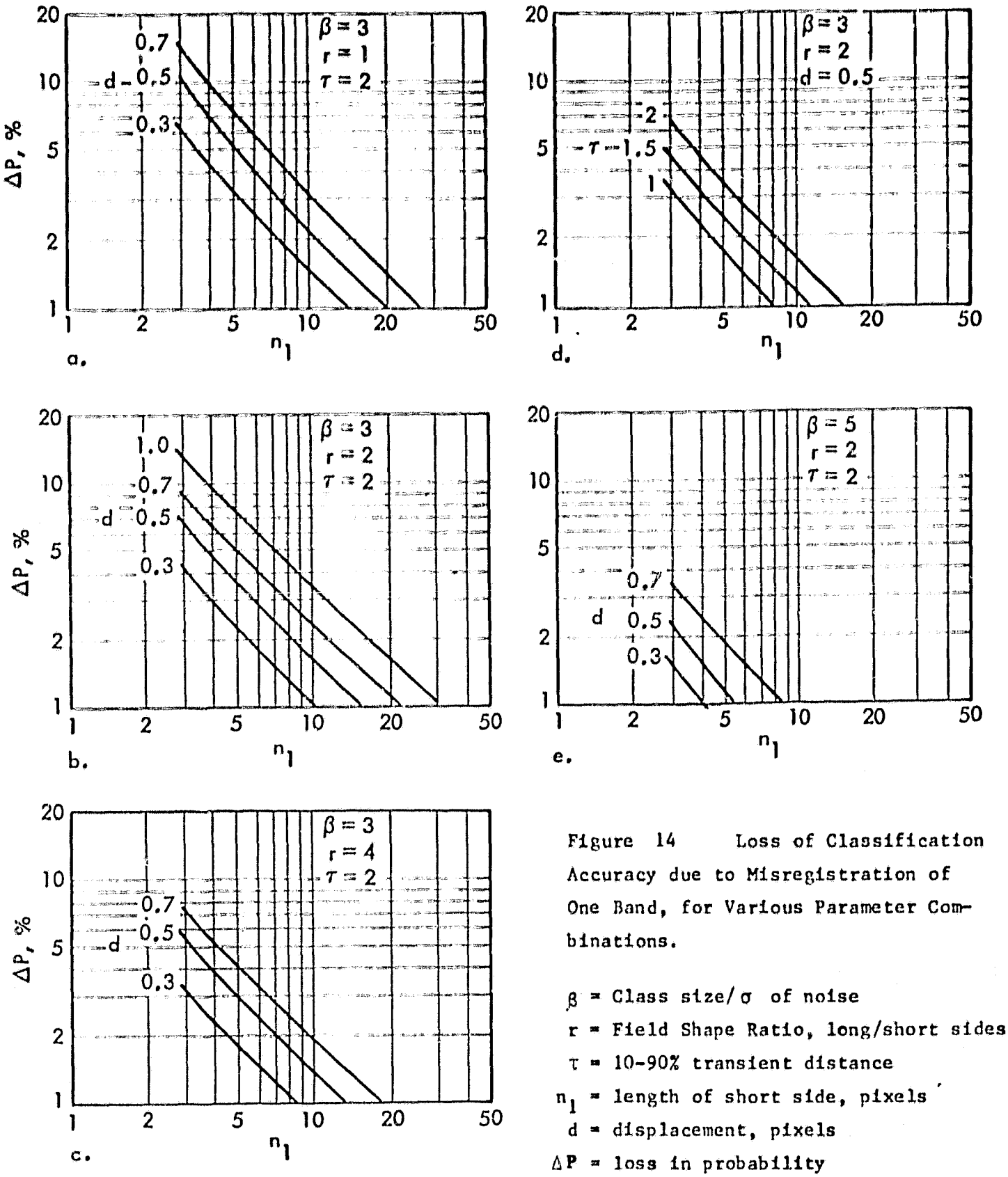

Figure 14 Loss of Classification Accuracy due to Misregistration of One Band, for Various Parameter Combinations.

β = Class size/σ of noise

r = Field Shape Ratio, long/short sides

τ = 10-90% transient distance

n_1 = length of short side, pixels

d = displacement, pixels

ΔP = loss in probability

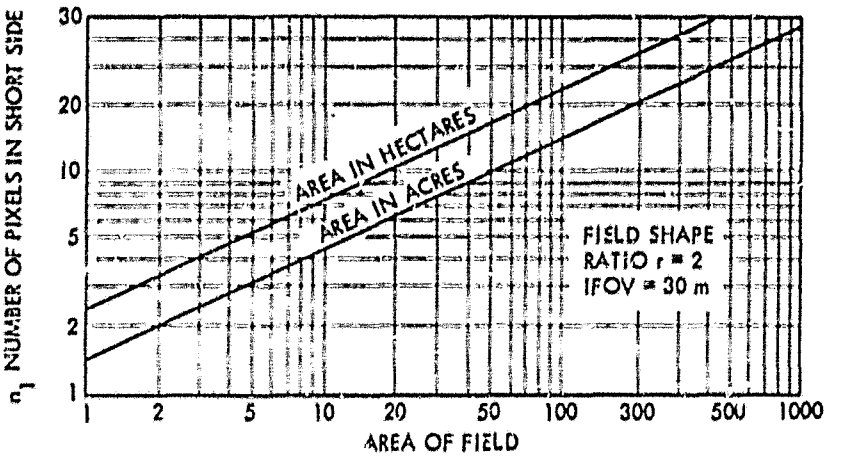

Figure 15 Field Area Scaling for 30 x 30 Meter Pixels and Shape Ratio r = 2.

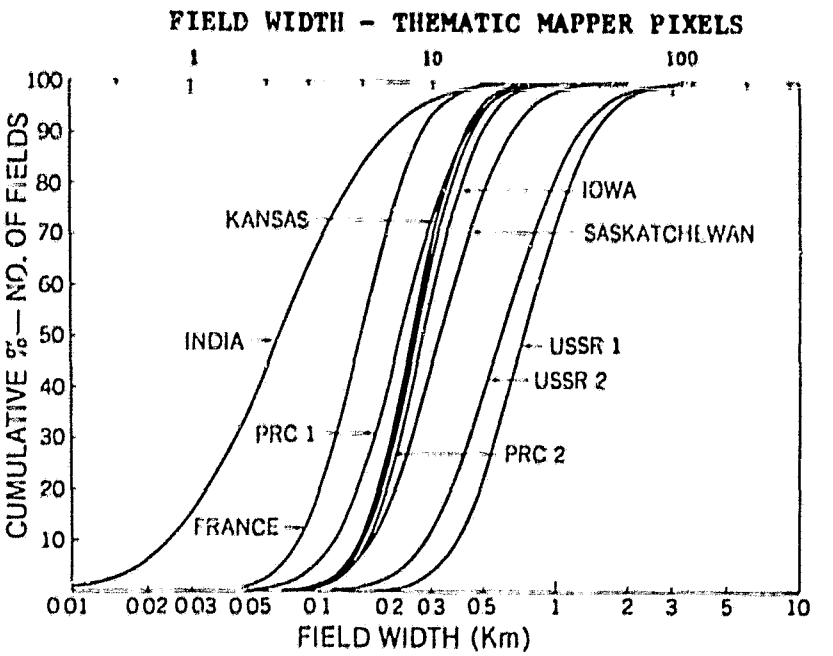

Figure 16 Cumulative Frequency Distribution (in %) of Field Width vs. Total Number of Fields. From Podwysocki, GSFC X-923-76-93

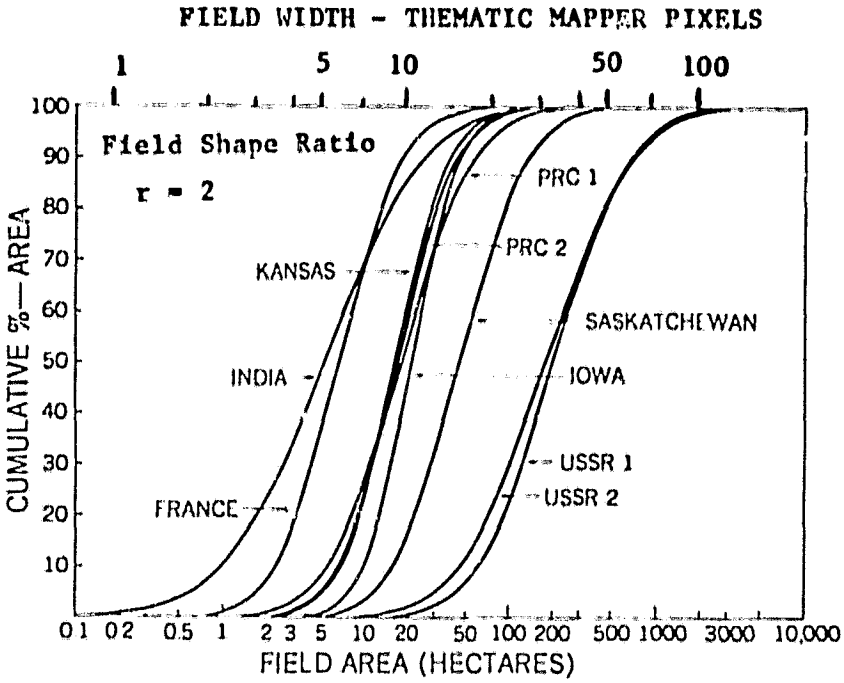

Figure 17 Cumulative Frequency Distribution (in %) of Field Area vs. Total Cumulative Area. From Podwysocki, GSFC X-923-76-93

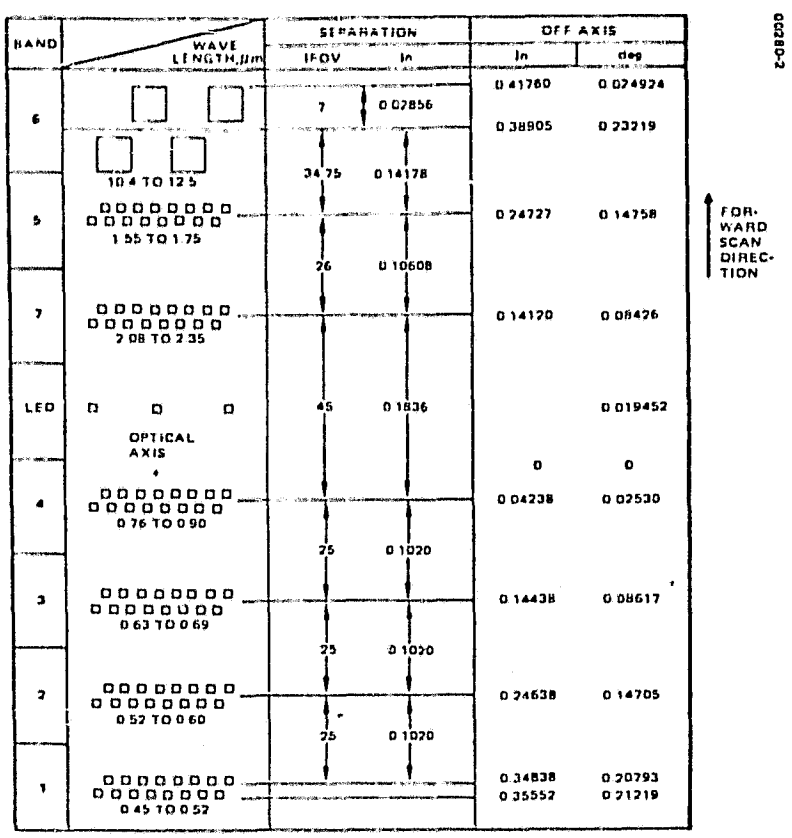

Figure 18 Detector Projection at Prime Focal Plane (From, Hughes, 1980)

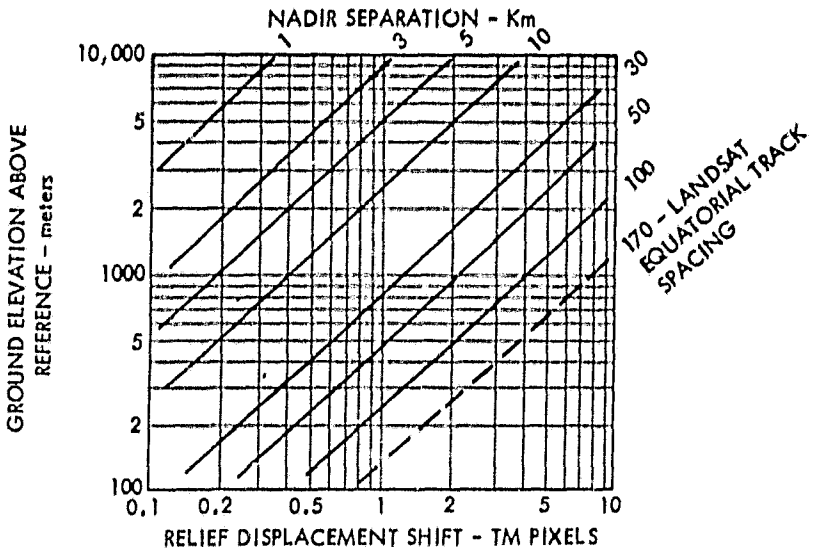

Figure 19 Relief Displacement Shift as a Function of Nadir Separation for the Thematic Mapper on Landsat D.

APPENDIX A - INTENSITY RESOLUTION

In the absence of all noise (i.e., no sensor noise and absolutely uniform scenes), finer intensity quantization would allow more subtle identifications. One estimate of usable quantization may be obtained by defining that "digitizing to m bits" means adjusting the quantization step size so that the scene plus sensor noise present causes the (m+1)th bit to be correct only 50% of the time (a subject for debate in itself). This is precisely the same problem discussed previously for the accuracy of multispectral classification and illustrated in Fig. 4 (Billingsley, 1975). Referring to that figure, we can see that 50% probability occurs with a $\beta \approx 1.5$ (for the (m+1)th bit) giving a $\beta \approx 3$ for the mth bit. For sensor rms noise of 0.5% (the TM specification) and no scene noise, the number of useful levels is $1/(3 \times 0.005) \approx 66$. On this basis, quantizing to 6 bits (64 levels) is justified, and the probability of zero error is about 0.7. This analysis may be modified if it is known that the noise varies with the brightness of the scene, but the approach is still valid.

Another estimate of the number of useful bits may be obtained by estimating the loss of accuracy of the classification caused by quantization error. Define the perfect sensor as having no random noise nor quantization error (i.e., an infinite number of bits). This will define

$$\beta_o = \frac{\text{class size} \cdot n}{\sigma_{\text{scene}}} \qquad \text{and} \qquad P_o = 10^{-0.4/\beta_o}$$

For the real sensor, $\beta < \beta_o$ because of the finite σ_{sensor} and $\sigma_{\text{quantization}}$. The new probability of correct classification P is related to P_o by:

$$P = P_o^{(\beta_o/\beta)}$$

The loss in classification accuracy $\Delta P = P_o - P$ thus depends on P_o and the ratio

$$\frac{\beta_o}{\beta} = \sqrt{1 + \frac{\sigma_2^2 + \sigma_3^2}{\sigma_1^2}}$$

where

σ_1 is the scene noise
σ_2 is the sensor random noise
σ_3 is the quantization noise.

The entire estimation boils down to estimating the P_o required, which sets β_o, and then partitioning the noise components to satisfy the desired ΔP. Note that unique explicit partitioning cannot be defined because neither the scene noise (pixel-pixel variation) nor the class-to-class separation, which influences the class size decision, can be controlled. However, to be useful, a classifier should have an accuracy in the 70-90% range, requiring $2.5 < \beta < 7$.

A plot of the loss in classification accuracy vs P_o is given in Fig. A-1, for the parameter families β_1/β and σ_2/σ_1. Noise allocation starts with the definition of the desired P_o and ascertaining that the required β_o can be obtained. Definition of the allowed ΔP determines (e.g., from

the graph) the allowed $\sigma_{sensor}/\sigma_{scene}$. An estimation of the scene noise for which the other conditions apply allows the calculation of the total sensor noise allowed. The final step is to partition this noise between sensor random noise and quantization noise.

For example, let P_o = 85%. Then β_o = -0.40/log(0.85) = 5.67. If we allow a 2% loss in accuracy due to the sensor, σ_2/σ_1 = 0.6 from Fig. A-1 or its related equation. If the expected scene for these accuracies has a noise (non-uniformity) σ_1 = 2%, the sensor can have a noise figure σ_2 = 0.6 x 2% = 1.2%. If the NE$\Delta\rho$ (random) of the sensor is expected to be 1%, the allowable $\sigma_{quantization} = \sqrt{1.2\%^2 - 1\%^2} = 0.66\%$. This can be met with 6-bit quantizing, for which $\sigma_{quantization} = 1/64\sqrt{12} = 0.45\%$. (Fig. A-2).

For the assumed conditions (β_o = 5.67 and σ_1 = 2%), the required class size must be at least 11.5% (5.67 x 2%) of full scale for individual pixel classification. If this causes confusion between classes due to overlap of class boundaries, several pixels must be averaged (i.e., $n > 1$) to reduce σ scene effective, or secondary criteria such as the per field classifier must be used.

Two final observations: (1) Increasing the number of bits of quantization produces improvements which asymptotically approach zero, as each successive bit reduces the step size by a factor of 1/2. (2) A scene having as little as 2% variation is a very uniform scene. Since this noise is rms'd with the sensor noise, it will overwhelm any but a very noisy sensor. Therefore, for purposes of multispectral classification, an extreme number of bits would seem to be unnecessary.

Essentially this same conclusion was reached by Tucker (1979) through a very different analysis route. He concluded that a 2% improvement could be obtained with 7 vs 6 bits, and a further 1% by 8 bits.

References:

Billingsley, "Noise Considerations in Digital Image Processing Hardware," Chaper in Picture Processing and Digital Filtering, T.S. Huang, ed., Springer-Verlag, Berlin 1975 and 1979.

Tucker, C. J., Radiometric Resolution for Monitoring Vegetation: How Many Bits are Needed?, NASA Technical Memorandum 80293, GSFC, May 1979.

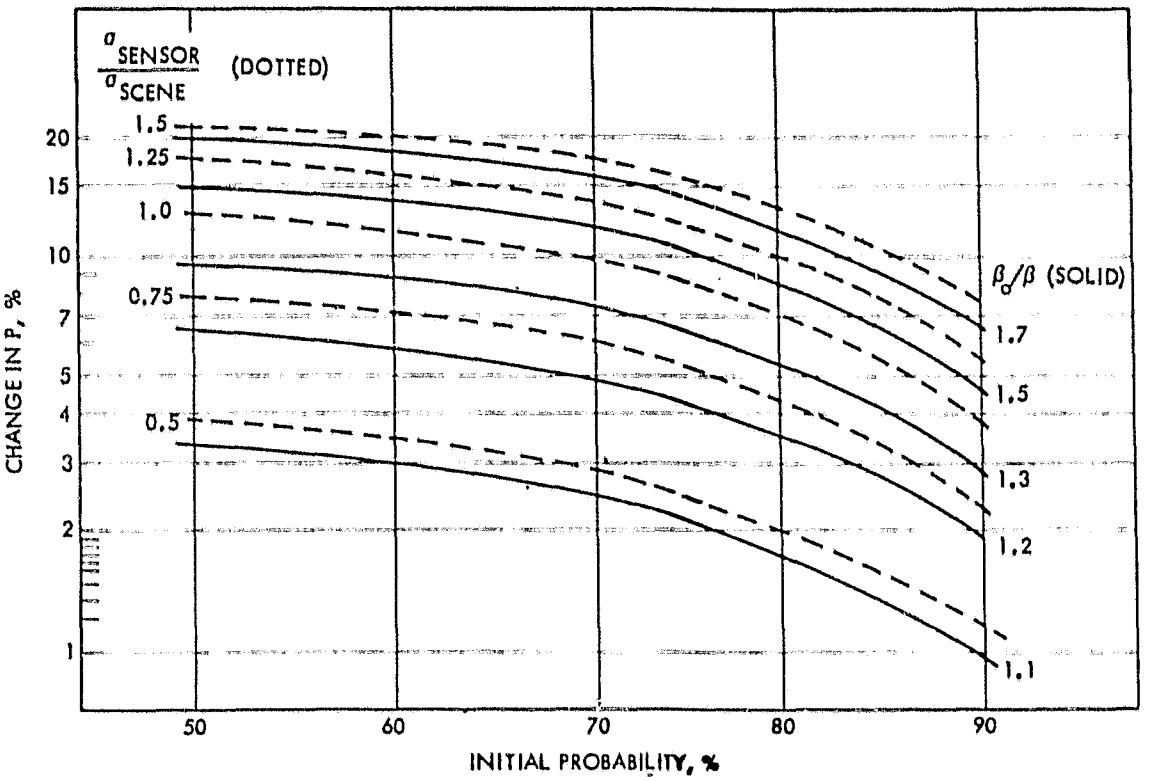

Figure A-1 Loss in Classification Accuracy due to Increase in Noise

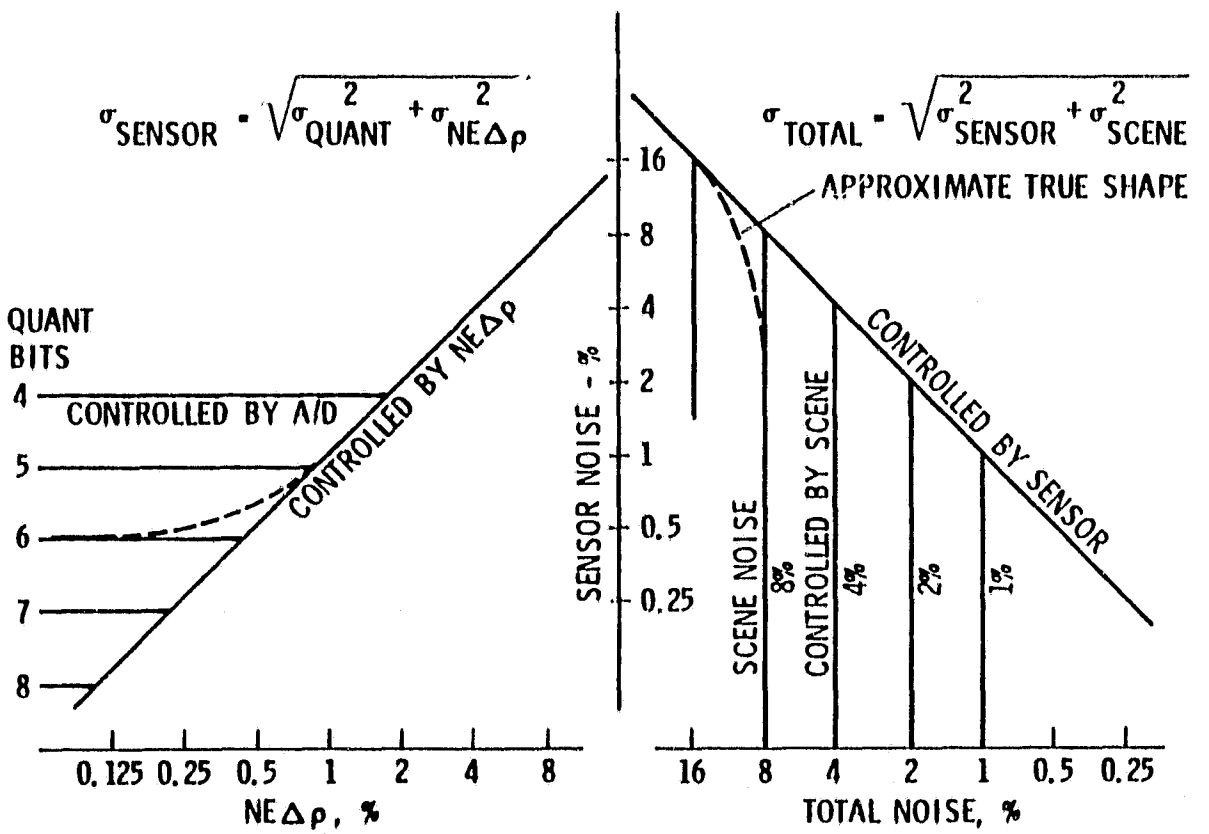

Figure A-2 Noise Contributions - Breakpoints

APPENDIX B TRANSIENT RESPONSE DISTANCE

The current specifications for the Thematic Mapper step response are:

> Scanning a step function (edge) of input radiance of any magnitude within the usable range of the TM shall produce a response satisfying the following criteria:
>
> a.) The overshoot/undershoot shall be limited to a maximum of 10% of the step size.
>
> b.) The step response for bands 1 through 5 and 7 shall be settled to within 1.5 percent of the final value within 30 microseconds, and to within 1 percent within 60 microseconds after start of response. Band 6 step response shall be settled to within 1.5 percent of the final value within 120 microseconds, and within 1 percent within 240 microseconds after start of response. Start of response is defined as the time when the response level change exceeds 2 percent of the step size.
>
> c.) The rise time for bands 1 through 5 and 7 shall be less than 20 microseconds. The rise time for band 6 shall be less than 80 microseconds. Rise time is defined as the time interval for the response to go from 2 percent of step size to the first point in time that the response is 2 percent of step size away from the final steady state value.
>
> d.) The variation of response time between channels of each band shall not exceed +- .5 microseconds and shall be characterized as "systematic" or "random." Response time is defined as the time difference between the 50% points of stimulus leading/trailing edge and the video channel output leading/trailing edge.

The critical portion of this specification for the present discussion is paragraph c). As the sample spacing for the TM is about 9.8 μsec, an equivalent statement for rise distance would be "...2% to 98% in 2.04 pixels." The optical blur, lens diffraction, detector size, electronic filter and atmosphere blur, convolved together, will provide the total transfer function for the system. Neglecting the atmosphere, the effects of the remainder may be estimated as follows:

The elements affecting the response in the along-track and cross-track directions are:

LENS/OPTICS	APERTURE		Along Track
LENS/OPTICS	APERTURE	SIGNAL FILTER	Cross Track

A rectangular aperture (FB-1) 30 x 30 meter as projected onto the ground is swept across track at uniform velocity. For development of the transient distance the sampling is immaterial, although sampling will be accomplished at one sample per aperture distance (IFOV). Real detectors may have an intensity response which is quite uneven across the face of the detector. This will cause the transient rise and the accompanying MTF to deviate from the ideal case. These effects will be ignored, and the aperture modeled as having uniform response. (Fig. B-4).

The optics are assumed to have a Gaussian point spread function with a standard deviation of about 6 meters. (Hughes has found that the precise shape of this function is unimportant.) (Figure B-2)

The total along track point spread function is the convolution of the aperture and optics functions, as shown in Figure B-3. The response of this combination to a step function of ground brightness is the convolution of this point spread function with the step. This will be a ramp of duration about equal to the time for the detector to sweep one IFOV, blurred by the optics.

In the across track (along sweep) direction, the electronic filter response further affects the rise time. In the Hughes simulation, the blurred ramp was input to the filter and the response measured. The results showed that, except for the case of an undercompensated filter, the output rise time was about 13 sec, or 1.33 pixels (10%-90%, from the graphs). The accompanying 2%-98% rise time was about 20 sec, the specification limit.

The related filter delay (in the Hughes simulation) was about 16 - 20 μ sec, depending on the specific filter. Variation in this delay between filters will cause a variation in the apparent position of field edges, both between detectors within one band and between bands. To minimize registration trauma, these should be matched. At the very least, the measured delays must be known to allow compensation.

References

Hughes, (1980), Thematic Mapper User Sensitivity Study Report, prepared for NASA GSFC, July 1980.

ERIM, (1976), "Investigation of Landsat Follow-on Thematic Mapper Spatial Radiometric and Spectral Resolution," by J.P. Morgenstern, R.F. Nalepka, E.R. Kent, and J.D. Erickson, April 1976, ERIM Report, 119300-10-F.

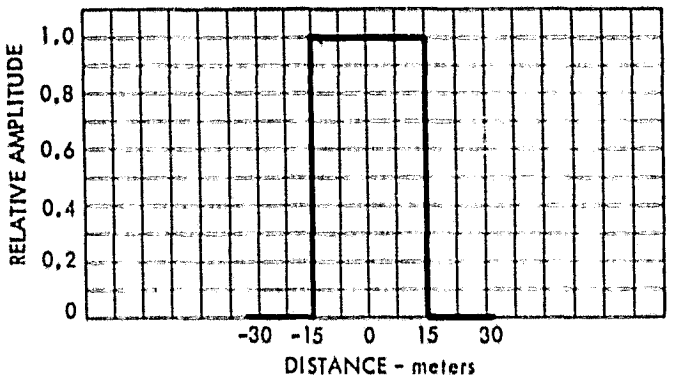

Figure B-1 ERIM TM Simulation - Scanning Aperture

Figure B-2 ERIM TM Simulation - Optics Gaussian Blur

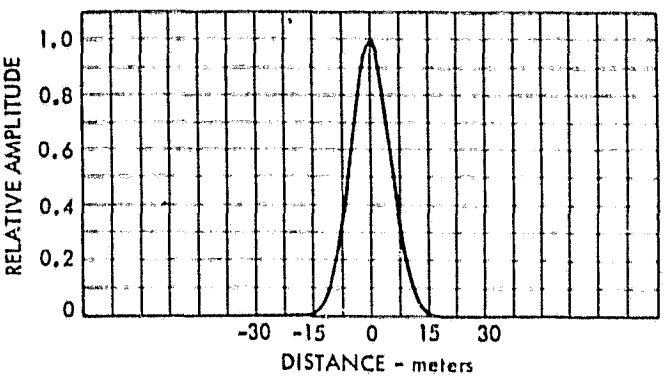

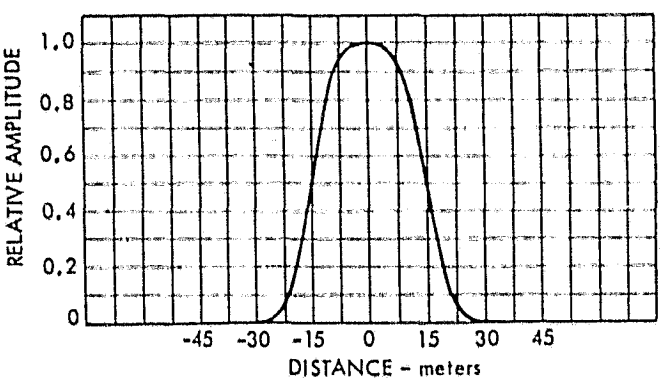

Figure B-3 ERIM TM Simulation - Along Track Spatial Weighting Function

Figure B-4 ERIM TM Simulation - Cross Track Transient Response

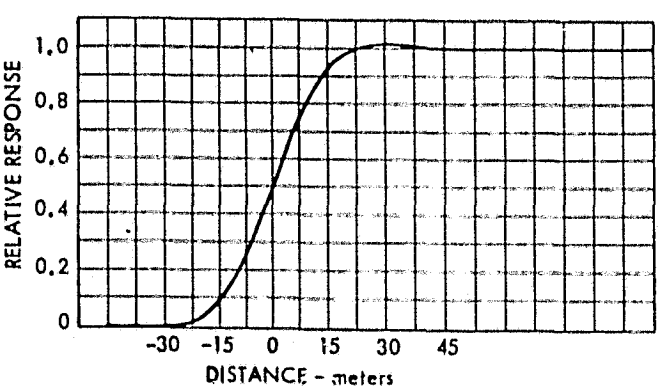

APPENDIX C - INTERPOLATION OR RESAMPLING

The problem of resampling arises whenever pixels are required in an output grid at locations different from where input pixels are located. Many methods of new pixel value generation are available; however, computation cost considerations tend to influence heavily the choice of method. The simplest method is called "nearest-neighbor resampling" and it assigns a value (dn) to a new output pixel location (i, j) according to the value $dn_{k,\ell}$ of the spatially nearest pixel (k, ℓ) in the input array to the precisely desired input location (x, y). The closest pixel (k, ℓ) is found by:

$$\left.\begin{aligned} k &= \text{integer part of } (x + 0.5) \\ \ell &= \text{integer part of } (y + 0.5) \end{aligned}\right\} \quad C\text{-}1$$

so the $dn_{i,j} = dn_{k,\ell}$.

This method preserves the exact value of pixels in the input data set, and thus introduces no new spectral classes; but it introduces spatial shift errors such that the local geometry may be inaccurate by up to $\sqrt{2}$ of the instantaneous field of view (IFOV), or the size of a pixel on the ground. Worse yet, the pixel from which the gray level is derived shifts suddenly in location from the pixel just before the correct resampling location (x, y) to the pixel just after it. This problem becomes critical during digital multitemporal picture comparisons because, while the registration of detail in the two images may be perfect in one location, elsewhere there is misregistration. Since the contribution of a given pixel is constant whenever the output sample is to be drawn from ± 1/2 pixel spacing, and zero outside of that range, the average frequency response is sinc x, with a first zero at one sample/cycle (Fig.C-1). It thus imperfectly filters the sampling sidebands, and has appreciable attenuation of the high baseband frequencies. The visible effect is the "blocky" appearance of images interpolated by this method. Nevertheless, for many purposes this interpolation is adequate, and may be accomplished with insignificant cost since only address-rounding is needed for each new pixel assignment.

A smoother approximation to the assumption of continuity is obtained when the adjacent pixel is allowed to influence the estimation of between-pixel values. When only the adjacent neighboring pixels are used, only a first-order (bilinear) interpolation is possible. In bilinear interpolation, $dn_{i,j}$ is found by using an interpolation scheme with the four nearest pixels surrounding the resampling location (x,y) to determine the dn at (x,y) (see Fig.C-2). If (x,y) lies between samples k and k + 1 and lines ℓ and ℓ + 1, then the gray level at (x,y) can be found by using:

$$dn_{xy} = (y-\ell)\left[(x-k)\,(dn_{\ell,k+1} - dn_{\ell k}) - (x-k)\,(dn_{\ell+1,k+1} - dn_{\ell+1,k})\right]$$

which reduces to

$$dn_{xy} = (x-k)\,(y-\ell)\left[dn_{\ell,k+1} + dn_{\ell+1,k} - dn_{\ell k} - dn_{\ell+1,k+1}\right] \qquad C\text{-}2$$

Since the contribution of a given pixel falls off linearly with distance to a distance ± one pixel spacing, (±a), the average frequency response (H) in one

dimension can be found by taking the Fourier transform of the triangular convolution kernel (h):

$$h_{bilinear} = \underset{-a\ +a}{\wedge} = \left(1 - \frac{x}{a}\right)_{x=0}^{a} + \left(1 + \frac{x}{a}\right)_{x=-a}^{0}$$

$$H_{bilinear} = \int_{-a}^{a} h e^{-2\pi f_x x} dx$$

where f_x is the frequency in the x direction and a is the sampling interval. Alternatively, $h_{bilinear}$ may be recognized as the convolution of two rectangular functions. In either case, the resulting frequency response is found to be $sinc^2 x$, with the first zero at one sample/cycle. Resultant images are much smoother than those from nearest-neighbor interpolation, have about 1/4 the mean-squared resampling error (Shlien, 1979) of nearest neighbor, and requires appreciably more computer time, primarily because of the four multiplications involved.

Accuracy can be improved further by increasing the number of pixels in the vicinity of the resampling location from the nearest 4 to the nearest 16 (4 x 4 matrix) or more. The additional points offer an opportunity not available using the simpler methods to shape the pass band by adjusting the relative contributions (via weighting factors) of the various pixels. Cubic methods have emerged as the most significant higher order resampling method and several variations exist. Classical cubic polynomial Lagrangian interpolation is the most common and produces a smooth resampled image with good frequency response. Sidelobes can cause overshoot; however, the cubic case is a good compromise between artifact introduction and computation cost. A spline function developed by Riffman (1973) has proven to be quite satisfactory in producing a reasonably shaped passband which provides some high-frequency enhancement:

$$\left.\begin{aligned} f_1(x) &= 1 - 2x^2 + |x| && 0<|x|\leq 1 \\ f_2(x) &= 4 - 8|x| + 5x^2 - |x|^3 && 1\leq|x|\leq 2 \\ f_3(x) &= 0 && 2\leq|x| \end{aligned}\right\} \quad C\text{-}3$$

This function and its passband are sketched in Fig.C-3 . It uses ± 2 neighbors for interpolation, has no contribution past 2 pixel spacings, and has continuous first derivatives. It has a mean-squared resampling error about 1/3 that of bilinear (Shlien, 1979), but requires four multiplies for each dimension.

Modifications of the cubic case have been designed to minimize undesirable characteristics [(Simon (1975), Riffman (1975), Tabor (1973)] while maintaining the four-multiply-each dimension per new pixel cost. Two examples will suffice.

1. By reducing the slope at the first zero crossing of the function of Eq. C-3 to one half, a new function (Eq. C-4) is produced having essentially the same transient rise distance but with less overshoot:

$$
\left.
\begin{aligned}
f_1(x) &= 1 - (1/2)[5x^2 - 3|x|^3] && 0 \le |x| \le 1 \\
f_2(x) &= (1/2)[4 - 8|x| + 5x^2 - |x|^3] && 1 \le |x| \le 2 \\
f_3(x) &= 0 && 2 \le |x|
\end{aligned}
\right\} \text{C-4}
$$

2. The functions of Eq. C-3 or C-4 are based on the requirement that they go through zero at a distance of 1 pixel from center, thus producing the negative lobe and the high-frequency enhancement. If, instead, the best approximation to a function represented by the samples is desired, and it is recognized that measurements made more than some distance away from a given pixel will have no influence on it, an interpolating function having limited support (i.e., local basis) and with the smoothest interpolation of all functions passing through the same set of points is desired. For equal spacing of the measurements, such a function is the cubic B-spline (Hou and Andrews, 1978), having continuity in the function and its first two derivatives at the knots (the sample points), zero slope at the center and at the second knot, zero amplitude past the second knot, and a summation of contributing, overlapping splines equal unity. Invoking these conditions, the cubic B-spline is found to be (symmetrical around x=0):

$$
\left.
\begin{aligned}
f_1(x) &= (1/6)\ [3|x|^3 - 6x^2 + 4] && 0 \le |x| \le 1 \\
f_2(x) &= (1/6)\ [-|x|^3 + 6x^2 - 12|x| + 8] && 1 \le |x| \le 2 \\
f_3(x) &= 0 && 2 \le |x|
\end{aligned}
\right\} \text{C-5}
$$

A plot of this function is given in Fig.C-4. It can be shown (Peyrovian, 1976) that for sampling near the Nyquist rate, the cubic B-spline is the optimum interpolator. Other interesting properties of spline interpolation are given in LaFata and Rosen (1970), Curry and Schoenberg (1966), Hou (1976) and references therein.

Finally, by using more than ± 2 samples to determine the interpolation function, higher order functions may be produced having less mean-squared resampling errors than any of the above (Shlien, 1979). However, recognizing that Landsat, for example, has a finite amount of sensor noise, the utility of reproducing this noise with greater fidelity is suspect, and the higher order interpolators have not found widespread use.

SOME GENERAL COMMENTS ON INTERPOLATION:

1. Cubic convolution in the orginal sense generates overshoot on abrupt borders with high brightness differences. This is the reason that the modified coeffficients were derived. They have been largely ignored to date.

2. Cubic convolution causes the apparent spread of small features. But small features can only be accurately located (within pixel) through the estimated continuum. Very small features such as Evans' (1974) mirrors do not satisfy the basic Nyquist criterion and should not be used as a surrogate for the world. To the extent that they are important, they must be evaluated independently of classification accuracy and precision spatial location.

3. Nearest neighbor registration will cause discontinuities in the location of edges. This is particularly disconcerting for features which lie at a small angle with respect to the scanning raster. Small rotations will be continually encountered in registering the nominal overlay images of a given WRS. Interpolation minimizes these discontinuities.

4. Jayroe (1976) illustrated the severe moire effect caused in the visual appearance of images registered by nearest neighbor. This visual effect is minimized with interpolation.

EFFECTS ON CLASSIFICATION ACCURACY

The discussion so far has concentrated on the ability of the interpolator to generate the continuum of which the original pixels were samples, after which the continuum was resampled to estimate the dn value of a sample which might have been acquired at an inter-original-pixel location. This process (except for the nearest neighbor process) generates intermediate dn values, and in general produces a smoother image. In the context of misregistration, the tradeoff is one of locating an original pixel at the wrong location (nearest neighbor) vs locating a new pixel with its attendant new dn value at the correct location (interpolator).

The original pixels are not independent, as shown by the transient distance being in the amount of about 1.5 pixels. The additional correlation produced by the filtering of the interpolator will be minimal, as the basic Nyquist sampling spacing is approximately satisfied. However, if contiguous training samples are assumed to be independent, the correlation will cause the training class spread to be underestimated. This in turn may cause the class decision limits to be changed, with a resulting change in β. At the same time, however, the filtering will reduce the field-interior noise, so that for reasonably uniform areas the choice of interpolation algorithm will be second order.

In Appendix D the conditions for an unbiased field area estimator are derived to be that the decision level should be midway between the brightnesses of the two fields on either side of a boundary. In this case, the new dn levels produced at borders using an interpolator will be picked up anyway, and their presence would seem to be inconsequential. If the decision levels are set for classification of the field materials, in general they will not be at the midway point. In this case, the new dn levels may well fall between the levels as defined for the adjoining field materials, and may therefore not be recognized. However, in this case, many of the true pixels, having border brightness changes due to the sensor spread function anyway, will also be lost. Nearest neighbor warping would seem to have a slight advantage in not producing the additional filtering. Once classified, only nearest neighbor warping can be used unless careful definition of proportion estimates are made for fractional pixels. The nearest neighbor pixels will have positional errors relative to other spacecraft passes due to the inability to locate them precisely onto the reference grid. These positional errors require that an estimation of the boundary position be made subsequent to classification; for multitemporal overlay the fractional pixel errors will counteract the slight advantage of no filtering.

APPENDIX C
REFERENCES

Curry, H.B. & Schoenberg, I.J., 1966. On Polya Frequency Functions IV. "The Fundamental Spline Functions and Their Limits," Jour d'Analyse Mathamatique (Jerusalem) Vol 17, P. 71.

Evans, W.R. (1974), Marking ERTS Images with a Small Mirror Reflector, Photogrammetric Engineering, Vol. 40, p. 665.

Goetz, A.F.H, etal (1975), Application of ERTS Images and Image Processing to Regional Geologic Problems and Geologic Mapping in Northern Arizona, JPL Report #32-1597, May 1975.

IBM: Ferneyhough, B.G. (1977), "Resampling Study, Final Report, Contract #NAS5-21865, January 1977.

Jayroe, R.R., Jr. (1976), Nearest Neighbor, Bilinear Interpolation and Bicubic Interpolation - Geographic Correction Effects on Landsat Imagery, NASA Technical Memorandum TMX-73345, Marshall Space Flight Center.

Hou, H.S., 1976. "Least Squares Image Restoration Using Spline Functions," USCIPS Report 650, Univ. So. Calif., Los Angeles, Ca., Feb. 1976.

Hou, H.S. & Andrews, H.C. (1978). Cubic Splines for Image Interpolation and Digital Filtering, IEEE Trans ASSP-26, Dec. 1978.

LaFata, P. & Rosen, J.P., 1970. "An Interactive Display for Approximation by Linear Programming," Comm of the ACM, Vol 13 #11, Nov. 1970.

Peyrovian, M.J., 1976. "Image Restoration by Spline Functions," USCIPI Report 680, Univ. So. Calif., Los Angeles, Ca., August, 1976.

Rifman, S.S., "Digital Rectification of ERTS Multispectral Imagery," Proc. of Symposium on Significant Results Obtained from the Earth Resources Technology Satellite-1, NASA Pub. SP-327, Mar. 1973, pp. 1131-1142.

Riffman, S.S., Allendoerfer, W.B., McKinnon, D.M. and Simon, K.W., 1975. "Experimental Study of Digital Image Processing Techniques for ERTS Data-Task 1 Final Report," Report #26232-6001-RU01, TRW Systems, Redondo, Beach, CA., Jan. 1975.

Shlien, S., 1979. "Geometric Correction, Registration and Resampling of Landsat Imagery," Canadian Jour Rm. Sens., V5 #1, May 1979, p. 74.

Simon, K.W., 1975. "Digital Image Reconstruction and Resampling for Geometric Manipulation," IEEE Sympos. Machine Processing of Remotely Sensed Data, June 1975, p. 3A-1.

Tabor, J.E., 1973. "Evaluation of Digitally Corrected ERTS Images," Third ERTS Sumposium, Vol. 1, NASA SP-351, Dec. 1973, p. 1837.

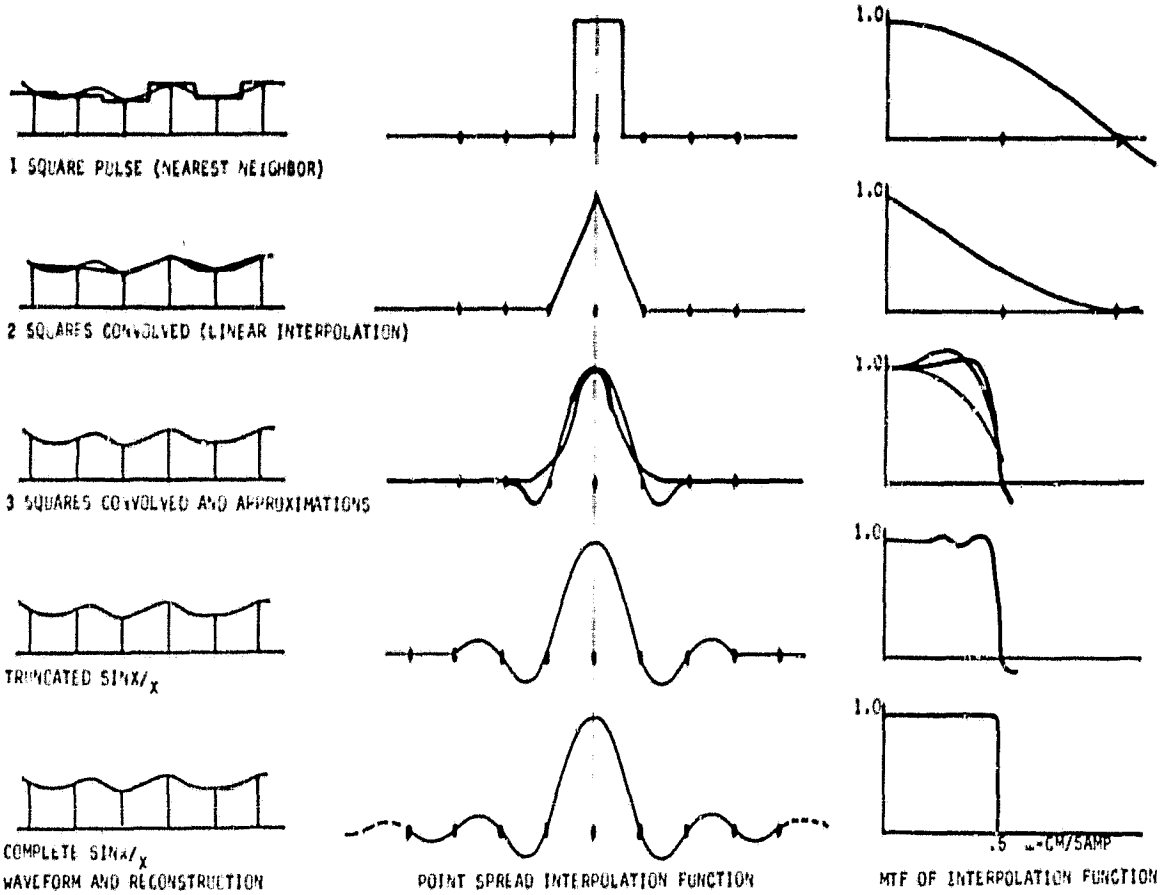

Figure C-1 Various Interpolation Functions and Their Frequency Response Curves

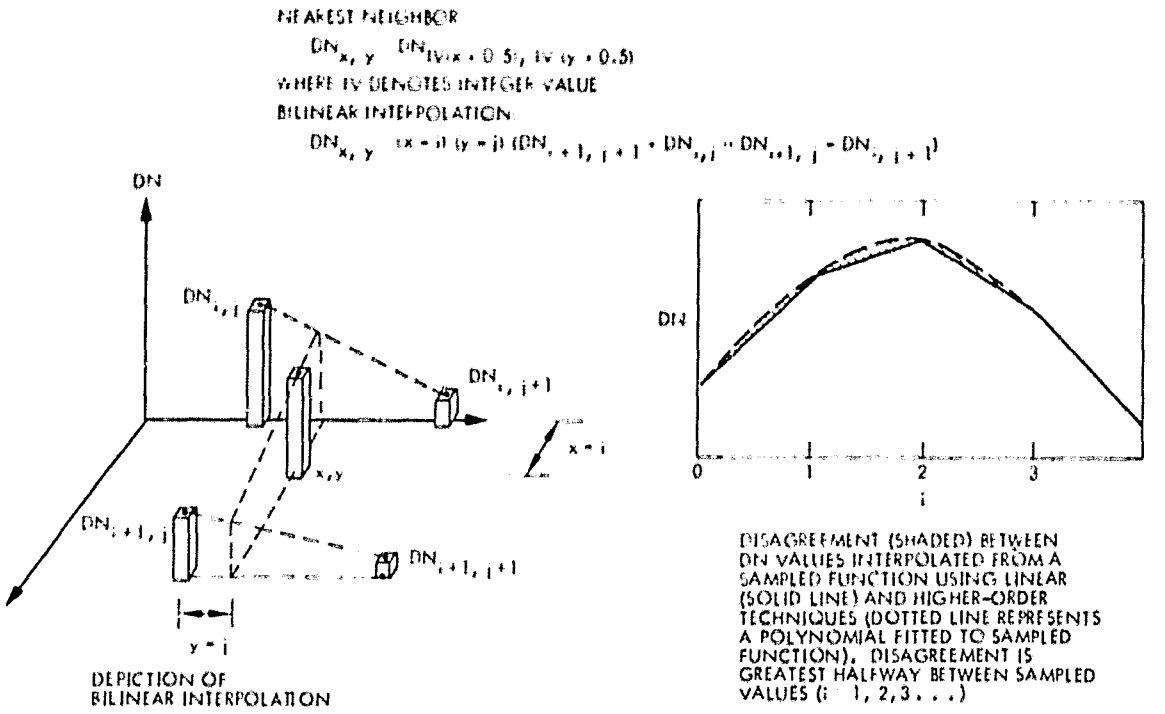

Figure C-2 Nearest Neighbor and Bilinear Interpolation Resampling Techniques. From Goetz et al, 1975

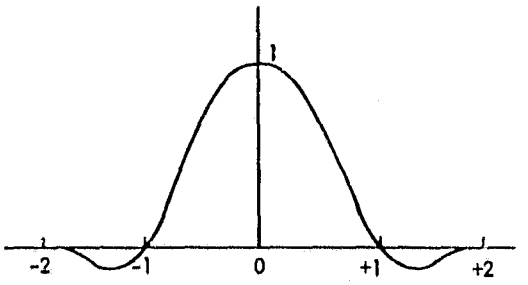

Figure C-3 TRW Cubic Convolution Spline

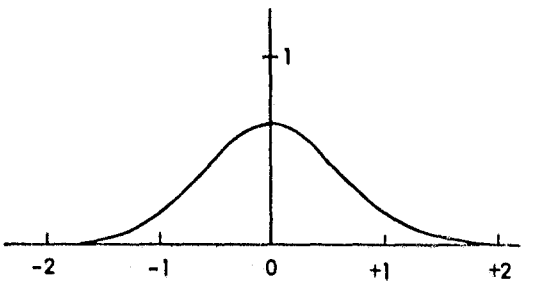

Figure C-4 Cubic B-spline

APPENDIX D - LOSS OF BORDER PIXELS

The progressive shift in the average brightness of a group of pixels as the group approaches a border (Figure 8-b) may be redrawn as Figure D-1. The class limit positions here are considered to shift with relation to the (noisy) group average brightness. The noise distribution, which in reality deviates toward bimodal (with mixtures more or less 50-50) and then back to Gaussian (from the adjacent field as it contributes the majority of the area), will be left as Gaussian for this analysis. Taking the σ of the group average as reference, a change in σ is reflected as an apparent change in class size. The right part of Figure D-1 indicates the locations of the class extent with various amounts of brightness offset (shift due to the border effect), scaled as fractions of the class size S. The upper and lower limits of the class, after offset, are the limits between which the fractional part of the Gaussian noise area is calculated. The result of the area calculation is given in Table D-1:

Offset xS	Corrected Area β=3	5	7
Zero	.866	.988	1.000.
1/8	.839	.969	.996
1/4	.761	.894	.960
3/8	.642	.734	.809
2/4	.500	.500	.500
5/8	.354	.266	.191
3/4	227	.106	.040
7/8	.130	.030	.004
4/4	.067	.006	
9/8	.031		
5/4	.012		

Table D-1. Fractions of the total area under the noise curve vs amounts of brightness shift scaled to class size S, for various β. Initial average brightness centered in the class.

These are the probabilities plotted in Figure 9-a. The shifts are from a starting position exactly centered within the class limits. As discussed in the body of the paper, this is optimistic, in that any group of field-interior pixels is not likely to be centered. But the field-interior pixels (zero offset) are the ones for which the probability of correct classification was calculated, leading to Figure 4. Therefore, the values of Table D-1 may be corrected by scaling to the field-interior values of Figure 4; this gives Table D-2 which has been plotted in Figure 9-b.

Offset Units of S	Corrected Areas β=3	β=5	β=7
0	.736	.832	.877
1/8	.713	.816	.873
1/4	.646	.753	.842
3/8	.545	.618	.710
1/2	.423	.421	.439
5/8	.300	.224	.168
3/4	.192	.089	.035
7/8	.110	.026	.004
1	.057	.005	
1-1/8	.026		
1-1/4	.010		

Table D-2. Fractions of the total area under the noise curve, based on groups of the interior pixels having a uniform probability of brightness.

Figure D-2 presents an expected transient response curve for the Thematic Mapper, as estimated by Morgenstern et al (ERIM Report 119200-10-F, April 1976). This curve is very close to that of a Gaussian impulse response function, and has a $t_{10-90} = 1$ pixel. Along-track and cross-track expected responses are almost the same, and will be considered the same for this analysis. Unity relative response in Figure D-2 is the transient total brightness shift T . What will be important is the shift as scaled to the desired class size S. Table D-3 relates the fractional response vs distance from the true border (50% point) for various T/S.

Distance From Border Pixels	Fractional Response	Shift From Full Response	Shifts in Units of S T/S=1	T/S=2	T/S=5
0	.5	.5	.5	1	2.5
.1	.6	.4	.4	.8	2.0
.2	.7	.3	.3	.6	1.5
.3	.78	.22	.22	.44	1.1
.4	.86	.14	.14	.28	.7
.5	.9	.10	.10	.20	.5
.6	.95	.05	.05	.10	.25
.8	.98	.02	.02	.04	.1
1.0	1.0	0	0	0	0

Table D-3. Relative transient response expected from the Thematic Mapper

The curves from Table D-3 are those of the right side of Figure 11.

BIAS IN FIELD SIZE ESTIMATION

The condition for no pixel loss is that the decision brightness for field boundary estimation should be midway between the brightnesses of the two fields on either side of the boundary. The sensitivity of the setting as it affects the apparent field size may be estimated as follows. (Figure D-3)

Define
- n_1 is the length in pixels of the short side of a rectangular field
- n_2 is the length in pixels of the long side of a rectangular field
- $r = n_2/n_1$ is the field shape ratio
- e is the distance in pixels of the loss in field size due to setting of the decision brightness
- T is the difference in brightness of the adjacent fields
- δ' is the decision brightness setting, away from the brightness of the field being considered
- δ is the decision brightness setting, scaled to units of T
- τ is the τ_{10-90} in pixels

The fractional area loss F is given by:

$$F = \frac{2n_2e_1 + 2n_1e_2 - 4e_1e_2}{rn_1^2} = \frac{2}{r}\left|\frac{n_2e_1 + n_1e_2}{n_1^2}\right. - \frac{4}{r}\left|\frac{e_1e_2}{n_1^2}\right.$$

For equal transient rise distance in both x and y, characteristic of the Thematic Mapper, $e_1 = e_2$, so that the fractional area loss becomes

$$F = \frac{r+1}{r}\left|\frac{2e}{n_1}\right. - \frac{1}{r}\left(\frac{2e}{n_1}\right)^2$$

Approximating the center portion of the transient rise by a straight line joining the 10% and 90% corner points (Figure D-3),

$$e = \frac{\tau}{T}\left(\frac{T}{2} - \delta'\right) \quad \text{and} \quad \frac{2e}{n_1} = \frac{2\tau}{n_1}\left(\frac{1}{2} - \delta\right)$$

giving for F:

$$F = \frac{r+1}{r}\left|\frac{2\tau}{n_1}\left(\frac{1}{2} - \delta\right)\right. - \frac{1}{r}\left(\frac{2\tau}{n_1}\right)^2\left(\frac{1}{2} - \delta\right)^2$$

The fractional area loss is zero when $\delta = 1/2$. The sensitivity of F to changes in the decision level δ is given by

$$\frac{dF}{d\delta} = -\frac{2\tau}{n_1}\left|\frac{r+1}{r}\right. \quad \text{at} \quad \delta = \frac{1}{2}$$

Figure D-4 shows the sensitivity ($dF/d\delta$) for two values of τ (1.0 and 1.5) and various values of the shape ratio, as functions of n_1, the number of

pixels in the short side of the field. The curves are generally hyperbolic due to the dominating influence of the $1/n_1$ term, with minor effects due to the shape ratio. However, maintaining the minimum τ is necessary; note that τ is the transient distance due to all causes.

Figure D-5 shows the fractional area loss for various parameters. Again, the $1/n_1$ term predominates the shape of the curves, so that errors are severe at small field sizes. Only at $\delta = 1/2$ are the errors eliminated. Given that $\delta = 1/2$ will not be the general setting of the decision level, minimization of F is accomplished by minimizing τ and by keeping δ as close to 1/2 as possible. The field ratio is of secondary importance, and in any event is not under the control of the sensor. Its effect may be estimated:

Recast the equation for F, letting $\frac{2\tau}{n_1}(\frac{1}{2} - \delta) = A$,

$$F = A + \frac{1}{r}(A - A^2)$$

Even for small fields, $A < 0.2$, so that A^2 may be ignored, giving

$$F \approx \frac{r + 1}{r} A$$

This is plotted in Figure D-6 for $\tau = 1.5$, with vertical scaling for two values of δ (0.3 and 0.4). All other things being equal, a change in shape from square ($r = 1$) to rectangular with $r = 4$ changes F by a ratio of 8/5. However, the actual magnitude of F will be small except for very small fields and δ deviating appreciably from 1/2.

Note that the distance δ is the same as one half of the class size of the discussion on pixels near borders; i.e., $\delta = S/2$.

RESEARCH NEEDED

The research problem implied by the $\delta = 1/2$ condition is:

- Automatic (at any speed, much less efficiently) blobbing is yet to be accomplished (Gupta and Wintz (1975) gave a start to this). The blobbing will in general produce fuzzy field boundaries. Continuity and closed boundaries must be assured.
- Vertices must be established to define boundary segments.
- For each spectral band, the correct intensity values of each set of field interior pixels must be established, after which the $\delta = 1/2$ condition may be defined for each segment.
- The best boundary position may now be found using $\delta = 1/2$. Since the decision levels will not be the same as those to be used for classification, they will not, in general, adequately characterize the ground cover material.
- Therefore, reclassification of the field interior pixels must be done to identify the materials. But since the field interiors are nominally uniform, a small number of surrogate pixels may suffice.

Reference:

Gupta J.N. & Wintz P.A. 1975 A Boundary Finding Algorithm and Its Applications, IEEE Trans on Circuits and Systems Vol. CAS-22 #4, P. 351.

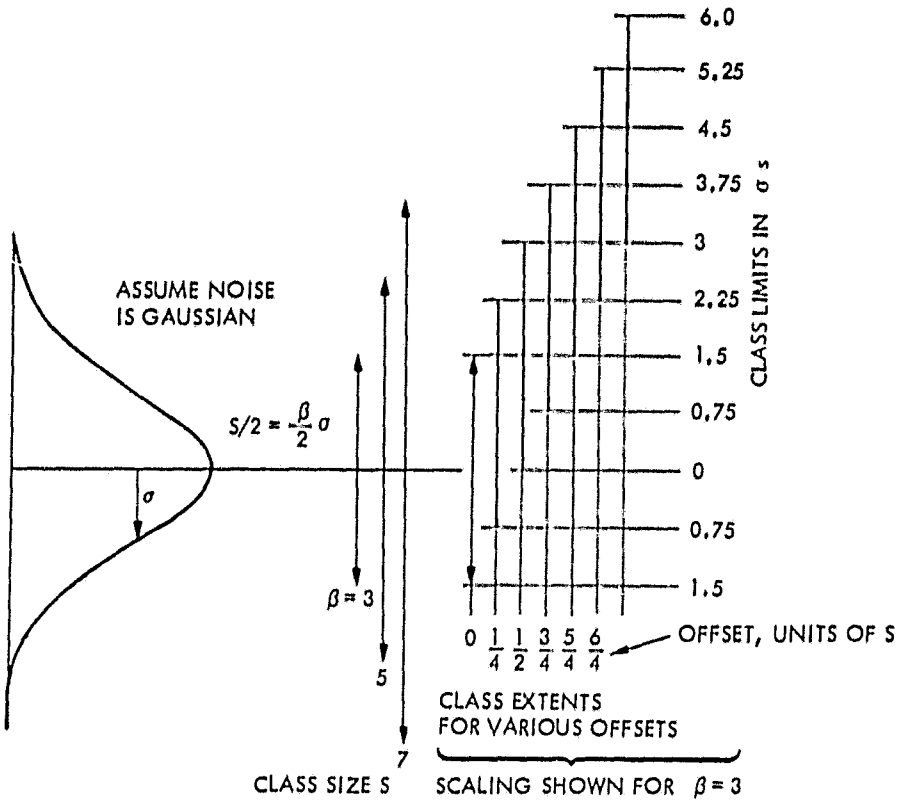

Figure D-1 Construction for Estimating the Fraction of Area Included under the Gaussian Noise Curve. The area is that which is included within the class boundaries; these boundaries move with respect to the noise curve as pixels approach the field borders.

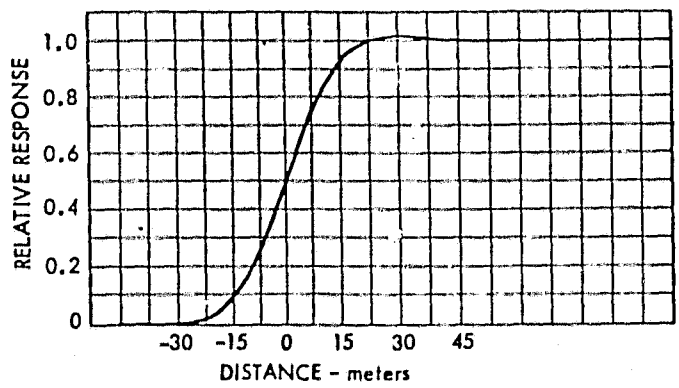

Figure D-2 Transient Response Estimated for the Thematic Mapper is Essentially zero to Full Scale in ± one Pixel. ERIM, 1976.

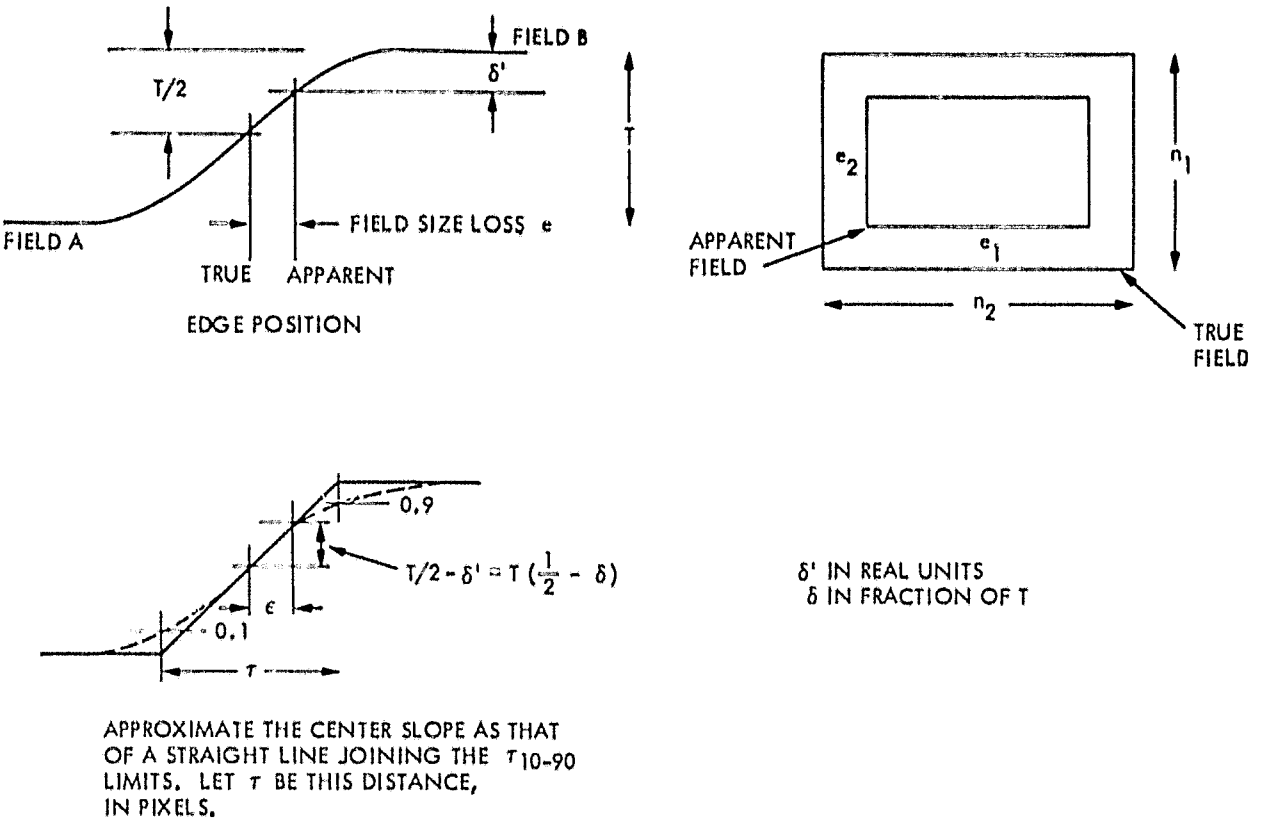

Figure D-3 Construction for Estimation of Loss of Field Size vs. δ/T

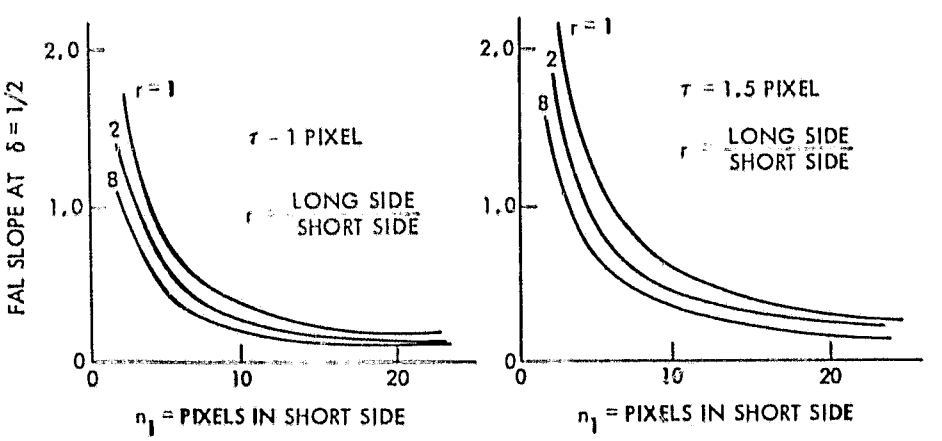

Figure D-4 Fractional Area Loss (FAL) Sensitivity near the Optimum Decision Level Setting ($\delta = \frac{1}{2}$) as a Function of the Number of Pixels in the Short Side (n_1).

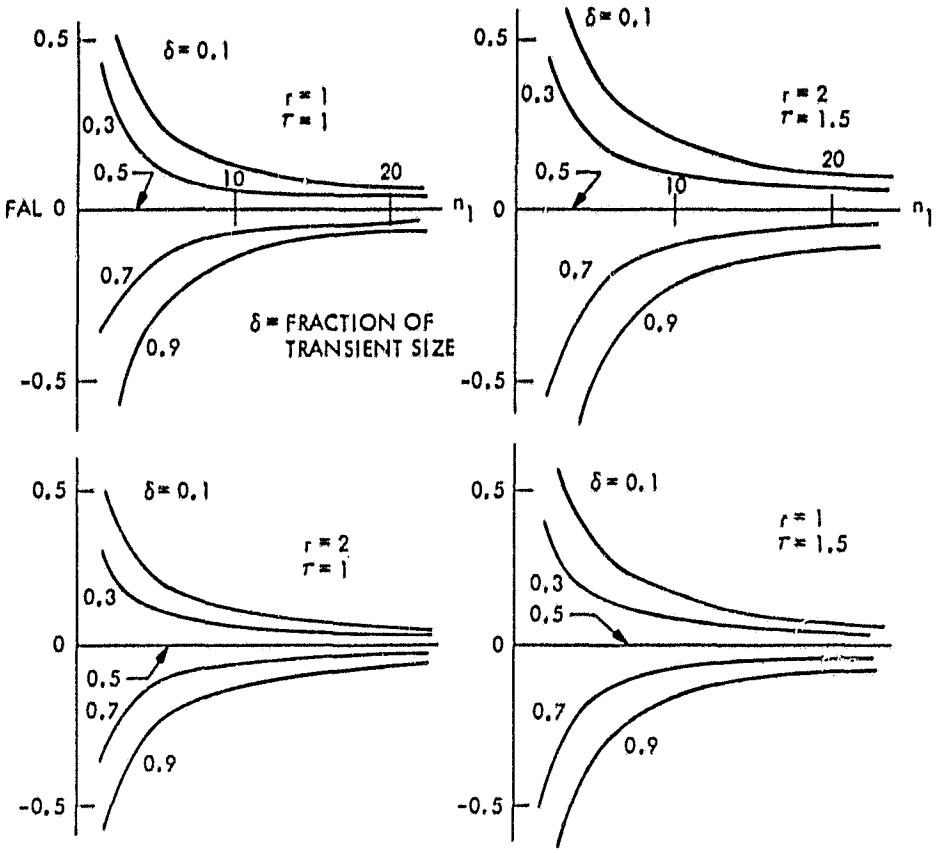

Figure D-5 Fractional Area Loss (FAL) for Various Parameter Values as a Function of the Number of Pixels in the Short Side (n_1).

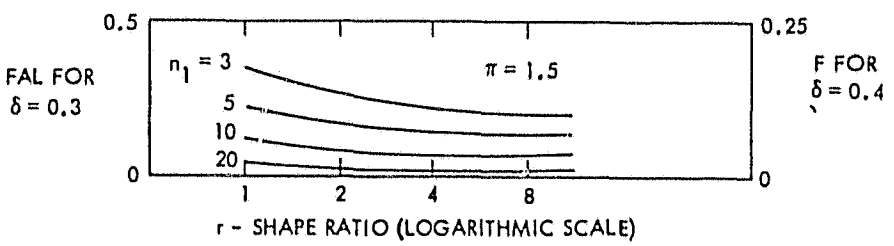

Figure D-6 Influence of Shape Ratio on Field Area Loss

APPENDIX E - TOTAL CLASSIFICATION EFFECTS

The total probability of correct classification is given by

$$P = \frac{1}{rn_1^2}\left(p_i n_i + p_{ib} n_{ib} + p_{ob} n_{ob}\right) = p_i f_i + p_{ib} f_{ib} + p_{ob} f_{ob} + p_{xb} f_{xb}$$

The fraction f of the total number of pixels in each zone are (Figure 12):

Interior	: $f_i = 1 - 4 \cdot \frac{r+1}{r} \cdot \frac{1}{n_1} + \frac{16}{r} \cdot \frac{1}{n_1^2}$	$n_1 \geq 4$
	$f_i = 0$	$n_1 = 3,4$
Inner Border	: $f_{ib} = 2 \cdot \frac{r+1}{r} \cdot \frac{1}{n_1} - \frac{12}{r} \cdot \frac{1}{n_1^2}$	$n_1 \geq 4$
	$f_{ib} = \frac{1}{n_1} - \frac{2}{rn_1^2}$	$n_1 = 3$
Outer Border	: $f_{ob} = 2 \cdot \frac{r+1}{r} \cdot \frac{1}{n_1} - \frac{4}{r} \cdot \frac{1}{n_1^2}$	$n_1 \geq 4$
	$f_{ob} = \frac{2}{n_1} + \frac{2}{r} \cdot \frac{1}{n_1^2}$	$n_1 = 3$
Exterior Border	: $f_{xb} = 2 \cdot \frac{r+1}{r} \cdot \frac{1}{n_1} + \frac{4}{r} \cdot \frac{1}{n_1^2}$	All n

These are plotted in Figure E-1 for r = 2, and the complete set of values is given in Table E-1. It can be seen from the table that the values for the average of all field sizes closely tracks the values for r=2. This ratio r=2 will therefore be chosen to represent the world. Verification of the adequacy of this choice may be discerned from the plot of Figure E-2, in which variation of r has little effect on the probability, as indicated by the curves for r=1 and r=8 being almost parallel, and close together.

With r fixed at r=2, attention may now be focused on the probabilities, to evaluate the sensitivity to T/S, τ, and β. The probabilities of correct classification for each zone are determined from Figure 10 for the set of parameters desired. These are listed in Table E-2 for various T/S, τ, and β. To evaluate the effect of β, intermediate values of τ, r, and T/S are selected, and p vs n_1 plotted for β = 3 and 5 (Figure E-3). Decreasing β has the expected effect of decreasing the probability of correct classification at any n_1. As the loss in p is about the same at all n_1, it is concluded that this loss is essentially independent of n_1. β = 3 will be used to represent the global situation.

Figure E-4 contains two plots, for different τ (1.5 and 2), of the probability vs n_1 for families of T/S. The exact shape of the curves

n_1	r=1			r=2				r=4			r=8			Average		
	i	ib	ob	i	ib	ob	xb	i	ib	ob	i	ib	ob	i	ib	ob
3	0	.111	.889	0	.222	.778	1.222	0	.278	.722	0	.306	.694	0	.229	.771
4	0	.25	.750	0	.375	.625	.875	0	.438	.562	0	.469	.531	0	.383	.617
5	.040	.32	.640	.12	.360	.520	.680	.160	.360	.460	.18	.390	.430	.125	.362	.513
7	.184	.326	.490	.306	.306	.388	.469	.367	.296	.337	.398	.291	.311	.314	.305	.381
10	.360	.28	.360	.480	.240	.280	.320	.540	.220	.240	.570	.210	.220	.488	.237	.275
15	.538	.213	.249	.636	.173	.191	.209	.648	153	.162	.709	.143	.148	.642	.171	.187
20	.640	.170	.190	.720	.135	.145	.155	.760	.117	.123	.780	.109	.111	.725	.133	.142
25	.706	.141	.154	.773	.110	.117	.123	.806	.095	.098	.823	.088	.089	.777	.108	.115

Table E-1 Fractions of total area in interior and borders

T/S	β	T=1			T=1.5			T=2			all T
		ob	xb	ib	ob	xb	ib	ob	xb	ib	interior
1	3	.72	.10	.736	.68	.14	.736	.645	.20	.732	.736
	5	.82	.02	.832	.785	.025	.832	.753	.07	.830	.832
	7	.837	0	.877	.86	.01	.877	.84	.04	.875	.877
2	3	.68		.736	.535		.736	.44		.730	.736
	5	.785		.832	.592		.832	.44		.828	.823
	7	.86		.877	.67		.877	.44		.872	.877
5	3	.45		.736	.09		.736	.01		.712	.736
	5	.45		.823	.03		.823	0		.815	.823
	7	.45		.877	0		.877	0		.870	.877
10	3	.07		.736			.732			.66	.736
	5	.02		.832			.830			.768	.832
	7	0		.877			.875			.85	.877

Table E-2 Zone Probabilities, from Figure 11

T/S = 1 Misregistration Loss = $f_{loss} \cdot P_{xb}$

		β=3 r=1 T=1	β=3 r=1 T=1.5	β=3 r=1 T=2	β=3 r=4 T=1	β=3 r=4 T=1.5	β=3 r=4 T=2	β=5 r=2 T=1	β=5 r=2 T=1.5	β=5 r=2 T=2.0
	P_{xb}	.10	.14	.20	.10	.14	.20	.02	.025	.07
d=.3	n_1= 3	.320		.064	.021		.042	.016		.032	.004	.005	.015
	4	.022		.044	.015		.030	.011		.022	.003	.004	.010
	5	.016		.032	.011		.022	.009		.018			.008
	7	.011		.022	.008		.016	.006	.008	.012			.005
	10	.007		.014	.005		.010	.004	.006	.008			.004
	15	.005		.010	.003		.006	.003	.004	.005			
	20	.003		.006	.002		.005	.002	.003	.004			
	25	.003		.005	.002		.004	.002	.003	.003			
d=.5	3	.053		.106	.035	.049	.070	.026		.055		.009	.024
	4	.036		.072	.024	.034	.048	.018		.037		.006	.017
	5	.027		.054	.018	.025	.037	.014		.029		.005	.013
	7	.018		.036	.012	.017	.025	.010		.020		.003	.008
	10	.012		.024	.008	.011	.017	.007		.013			.006
	15	.007		.014	.005	.008	.011	.004		.009			.004
	20	.005		.010	.004	.006	.080	.003		.006			
	25	.004		.008	.003	.005	.070	.003		.005			
d=.7	3	.072		.044	.048		.096	.036		.071		.012	.033
	4	.049		.098	.033		.067	.026		.051		.009	.023
	5	.037		.074	.025		.051	.020		.040		.006	.018
	7	.025		.050	.017		.035	.014		.027		.004	.012
	10	.016		.032	.012		.023	.009		.019			.008
	15	.010		.020	.007		.015	.006		.012			.005
	20	.008		.016	.006		.011	.004		.009			.004
	25	.006		.012	.004		.009	.004		.007			

Table E-3 Misregistration loss for various parameter combinations

depends on the precise shape estimated for the transient rise in Figure 10. Note that the T/S = 1 condition is the same as the $\delta = 1/2$ condition developed for the field boundary decision; this condition of no field size loss makes the probability of correct decision independent of r and n_1. The curves from the two plots in Figure E-4 closely superpose for high (e.g. ≥ 5) T/S, indicating that for the range of $1.5 < T < 2$, the resultant probabilities are independent of T. This occurs because the transient total shift is so high that recognition-or-not changes over a short range. For intermediate (e.g., 2) values of T/S, border pixels contribute a varying but significant part of the total; in this range, the transient distance T causes variation, and should be minimized to minimize the loss in accuracy for small fields.

MULTIPLE ACQUISITIONS

An acquisition will be considered to be one data set; that is, one spectral band. Again the basic model considered will be that in each band the β will cause a probability < 1 of recognizing a within-class pixel, and for trend and order of magnitude sensitivity analysis the covariance factors will be neglected. An output pixel grid defines the common matrix in which all images are analyzed and in which the "true" field position is defined.

For each acquisition 1, 2, 3, ...q, each pixel in the output grid will have an associated probability P derived as above. The resultant total P for the set of acquisitions is the product $P_1 P_2 P_3 \ldots P_q$ at each pixel. Denoting the mean P in the acquisitions at a given point as P_M,

$$P_1 P_2 \ldots P_q = P_M^q$$

This probability P_M^q may be carried through the zone analysis as above.

THE MISREGISTERED CASE (CONGRUENT FIELDS)

Figure E-5 is the construction for the case of misregistration of d pixels, assumed to be the same in both directions. No field shape or size distortion or rotation are modeled; shape errors (for one-band analysis) can be estimated as the algebraic average of deviation from the ideal position of the border pixels, and used as d. In this way the possible waviness in field shapes caused (for example) by the scan-line corrector errors can be accounted for. The construction is given in Figure E-7.

For calculation, the various zones are considered to be composed of components as shown. The loss in accuracy will be reflected in the lower probabilities in the components as they are seen in the misregistered position. Thus, the interior zone consists of a portion of the true field interior (a) and the component b, which is really in the true inner border transition zone. The remainder of the true field interior (i) is seen in the inner border. And so on.

Thus, the probabilities for the zones are:

Interior: $ap_i + bp_{ib} = (I-b)p_i + bp_{ib}$

Inner Border: $cp_{ib} + dp_{ob} + (i-b)p_i = (IB-a-b)p_{ib}+ap_{ob}+bp_i$

Outer Border: $ep_{ob} + fp_{xb} + (j-d)p_{ib} = (OB-f-d)p_{ob} + fp_{xb}+dp_{ib}$

External Border: $gp_{xb} + hp_o + (k-f)p_{ob} = (XB-h-f)p_{xb}+hp_o+fp_{ob}$
$p_o = 0$ (Outside)

Lost to Outside: $(\ell-h)=d\,[(r+1)n_1 + 4-d]$

The total probability is obtained by summing and collecting terms:

$$\begin{aligned}
\text{Interior} &: Ip_I - b(p_I - p_{Ib}) \\
\text{Inner Border} &: IBp_{Ib} + b(p_i - p_{ib}) - d(p_{ib} - p_{ob}) \\
\text{Outer Border} &: OBp_{ob} + d(p_{ib} - p_{ob}) - f(p_{ob} - p_{xb}) \\
\text{External Border} &: XBp_{xb} + f(p_{ob} - p_{xb}) - h(p_{xb} - p_o)
\end{aligned}$$

$$P = \underbrace{Ip_i + IBp_{ib} + OBp_{ob} + XB_{pxb}}\ \underbrace{-h(p_{xb})}$$

This is the probability of classification, with edge effects, before misregistration.

This is the additional loss due to misregistration.

Thus, the net effect (Figure E-6) is that the area ℓ, which was originally contributing with an effect p_{xb}, is no longer seen. In its place the area h, which contributes with an effect $p_o=0$ is now covered. Since h and ℓ are the same size, the net loss in probability is

$$h \cdot p_{xb} = d\left[(r+1)n_1 + 4 - d\right] p_{xb}.$$

The area of h, expressed as a fraction of the true field size rn^2, is:

$$f_h = d \cdot \frac{r+1}{r} \cdot \frac{1}{n_1} + (4d - d^2) \cdot \frac{1}{n_1^2}$$

The probabilities p_{xb} are estimated from Figure 10 (Table E-4):

T/S	β	τ = 1	τ = 1.5	τ = 2
1	3	.10	.14	.20
	5	.02	.025	.07
	7	0	.01	.04
2	3	0	0	0
	5	0	0	0
	7	0	0	0

Table E-4 Probability of Correct Recognition of pixels in the First Row (External Border, XB) Outside of the True Field Boundary

Combining the fractional area loss with the probabilities for various combinations of the other parameters gives the results of Table E-3, the total misregistration loss. This is the loss over and above the base accuracy attained with finite field sizes but no misregistration. The data in Table E-3 are graphed in Figure 14.

The use of the algebraic average for small values of wavy distortion of one band is developed from Figure E-8 (the global-value case of Figure 10). In the region of the field borders, each curve is more or less linear; for combined analysis of trends and sensitivity analysis, pixels further inside the border (than if registered) will have an increased probability, and those nearer or outside will have decreased probability. The (very) approximately linear change in P allows the algebraic average to be used, provided that commission and omission errors are considered to balance.

For more than one band analysis, because of the multiplication of the probabilities (per pixel) derived from each band, the lowest probability will predominate. In this case, the probability will drop as the number of (misregistered) bands increases, and commission and omission no longer balance. Because of the unpredictable relative locations of the offending border pixels, the rms combination of errors from all sources is appropriate.

MISREGISTRATION DUE TO SIZE AND RATIO (ASPECT) CHANGES

Size and aspect ratio changes can come about from several causes such as scan velocity or altitude changes, and if uncompensated can cause additional misregistration errors. The sensitivity to these can be analyzed using the constructions in Figure E-9. Progressive misregistration from a point of best registration will be caused by both causes (Figure E-9a); the modeling of this effect will be that first size changes $N = n'/n$ will cause a shift in points n to points n' both vertically and horizontally, and that changes in aspect ratio will cause further shifts in the horizontal position of vertical borders by changing the field shape ratios by the factor $R = r'/r$. The resulting shifts are;

$$\Delta n_v = (N-1)n_v \quad \text{and} \quad \Delta n_h = (NR-1)rn_v$$

In most analyses, this shift will be divided around the borders symmetrically as optimum field registration is accomplished (Figure E-9b). However, for analysis the construction of Figure E-9c is used. The sizes of the border position errors are (in pixels):

$$e_1 = (N-1)n_1 \quad \text{and} \quad e_2 = (NR-1)rn_1$$

Two cases must be distinguished (using scan velocity as a surrogate cause):

Case I: A slow scan decreases pixel spacing and puts more pixels into a given field. When these are placed into the output grid, the field appears stretched. The field as defined by the other (correct) bands now covers only part of the stretched field. The classification tends to see only interior pixels, and the accuracy will increase, ultimately reaching the field-interior accuracy.

The limiting field-interior classification accuracy will be reached when the field grows by four pixels in each direction. This occurs when

$$N = \frac{n + 4}{n} \qquad \text{provided that} \quad R \geq \frac{n + 2}{n + 4} .$$

Related to field sizes, the limits are:

Field Short Side, n_1, pixels	15	20	25	35	50	100	150	200
Minimun Limit, R	.985	.917	.931	.949	.936	.981	.987	.990
Maximum Reached when N =	1.267	1.200	1.160	1.110	1.080	1.040	1.027	1.020

It can be seen that for small fields, the accuracy increases for quite a wide range of R and N, but that for large fields, the limiting accuracy is reached with relatively small R and N errors. But at large n_1 the field total and field-interior accuracies are close, so that small accuracy changes will be produced.

Case II: A fast scan has the opposite effect, causing the field to appear smaller and the analysis pixels defined by the other bands now include more exterior pixels. The classification accuracy will decrease.

For fast scan, the smaller apparent field covers an area of

$$f_i = \frac{r'(n'_1)^2}{rn_1^2} = RN^2 \qquad \text{(Interior)}$$

Fractional Areas:

$$f_{xb} = \frac{2Nn_1 + 2NRn_1r + 4}{rn_1^2} \qquad \text{(External Border)}$$

The total expected probability is

$$P_{tot} = f_{i}P_i + f_{xb}\, P_{xb} .$$

This can be approximated for the assumed shape ratio r = 2 and N somewhere near 1:

$$P_{tot} \approx RN^2 p_i + \left[\frac{1 + 2RN^2}{n_1} + \frac{1}{n_1^2}\right] P_{xb}$$

Since the external border pixels are now included within the analyzed field, but with a low probability (See Table E-4), the fractional area RN^2 represents approximately the fraction of the basic field-interior accuracy to be expected. Since the total size shrinkage (in pixels) is small for small n_1, onlyar larger n_1 need be considered, and the 1/ term may be dropped. Further, for RN^2 near 1, the first term in the square brackets approaches $3/n_1$. Thus the total probability may be approximated by

$$P_{tot} \approx RN^2 p_i + \frac{3}{n_1} P_{xb} .$$

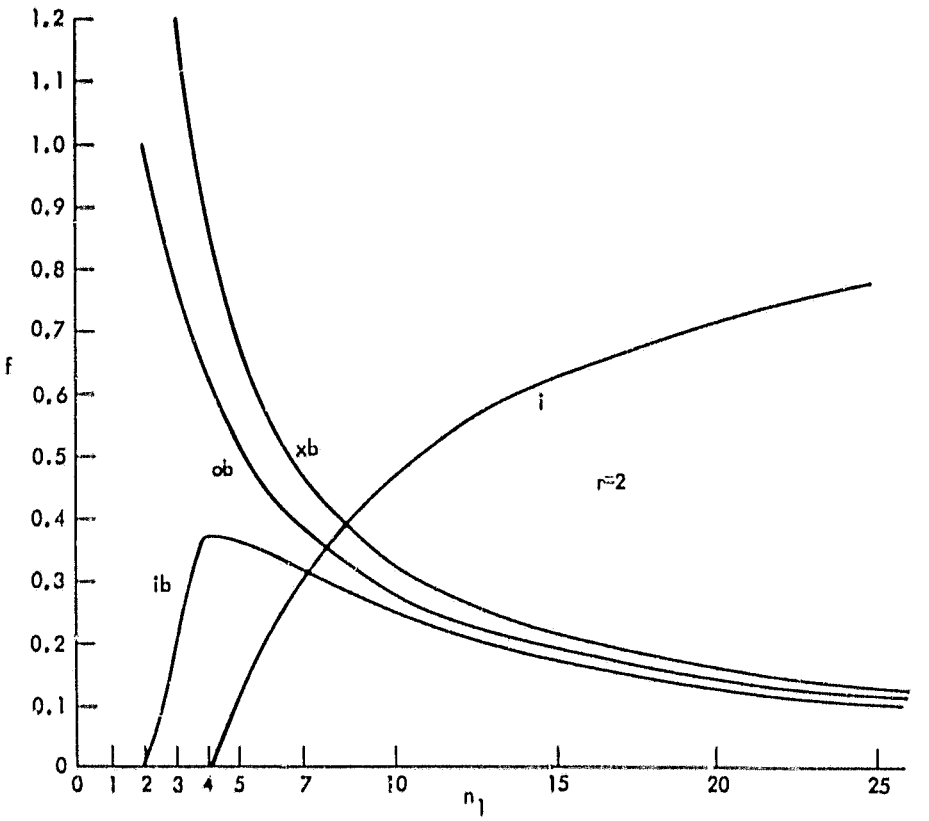

Figure E-1 Fractional Amounts (f) of Total In field Pixels in The Borders and Interior.

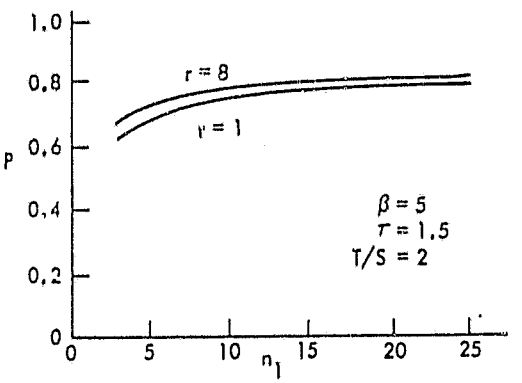

Figure E-2 Variation of Shape Ratio r has Small Effect on p.

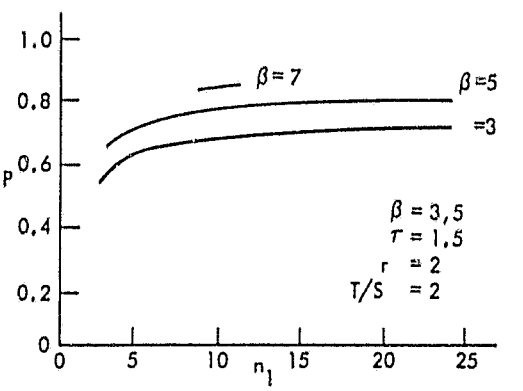

Figure E-3 Effect of Variation of β on p is relatively constant for all n_1.

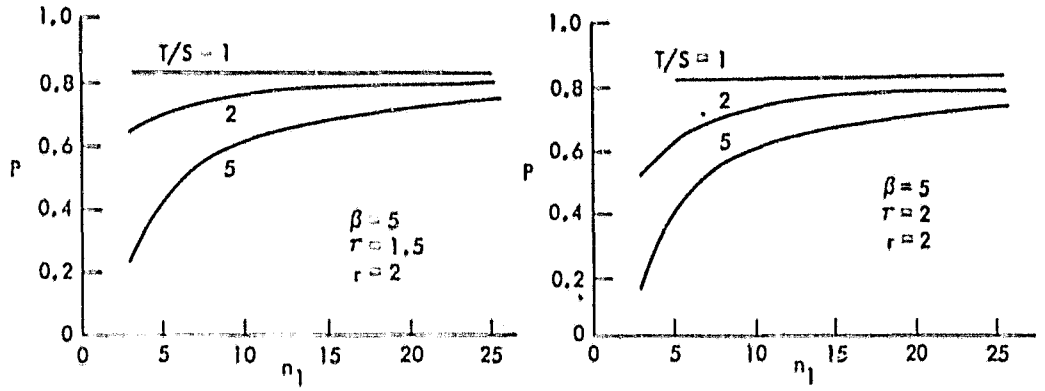

Figure E-4 Variation of Probability for Different Values of T/S

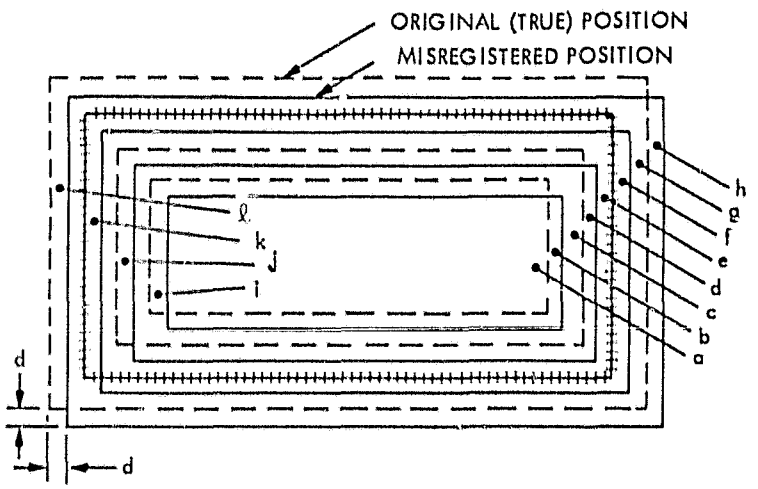

Area i = area b
j = d
k = f
ℓ = h

I	Interior	a + b
IB	Inner Border	c + d + i
OB	Outer Border	e + f + j
XB	External Border	g + h + k
L	Lost to outside	ℓ

Figure E-5 Component Areas for the Misregistered Case

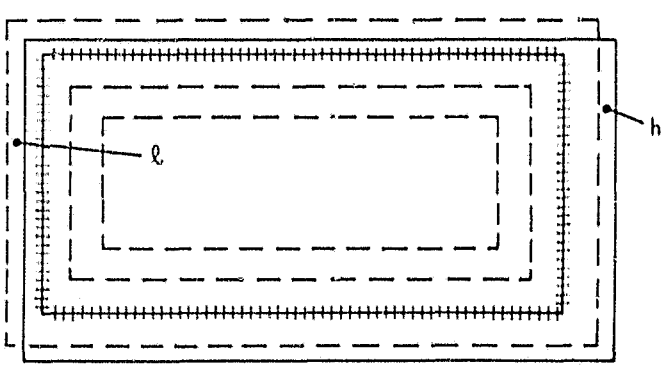

Area ℓ = $d\left[(r+1)n_1 + 4 - d\right]$

Figure E-6 The only net Loss due to Misregistration is the area ℓ

1.

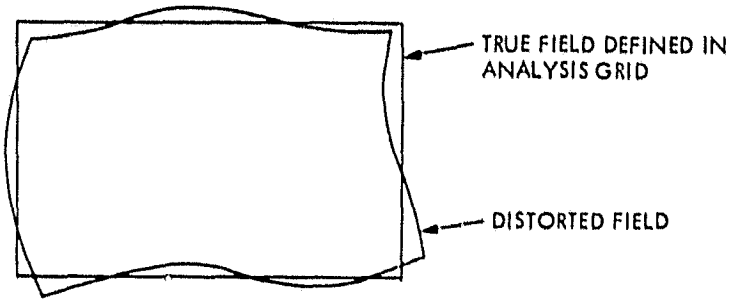

Figure E-7 General Case of Distorted Fields

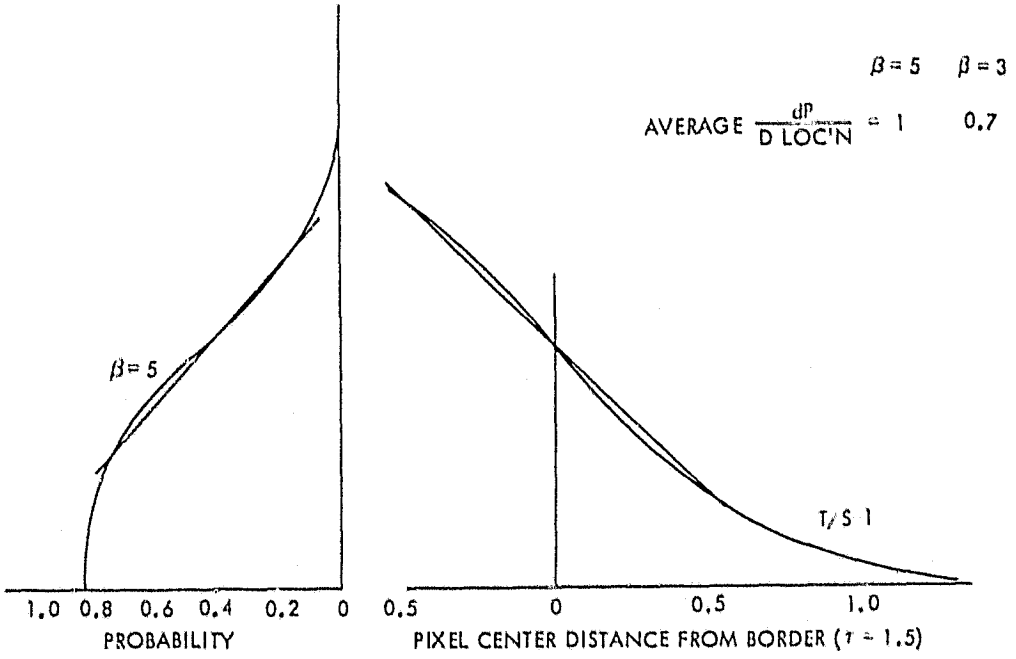

Figure E-8 Edge Pixel Classification Accuracy (From Figure 10) and Linear Approximations

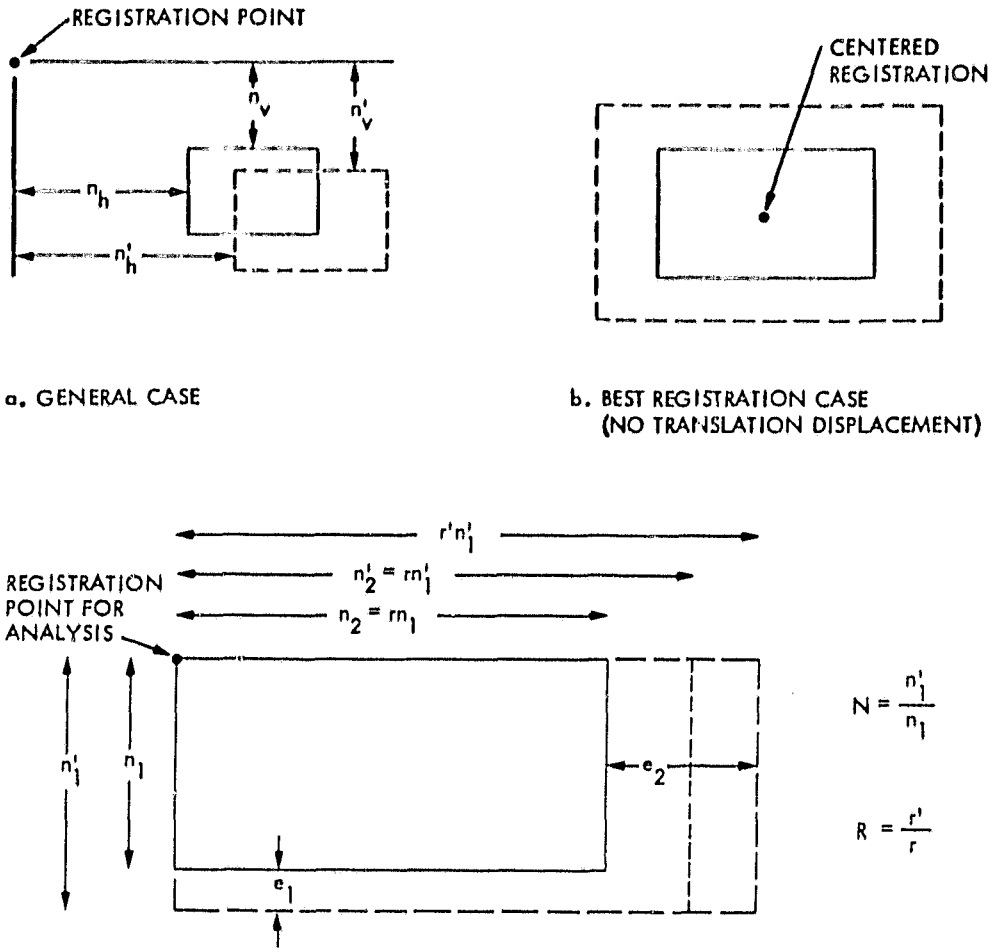

Figure E-9 Construction for Estimating Misregistration Caused by Size and Aspect Ratio Errors.

APPENDIX F - RELIEF DISPLACEMENT

The scenario used for relief displacement estimations is that for each image, the system processing will estimate a best fit plane using the ground control points, and correct the data to this. Deviations in the altitude of intermediate image points from this plane will cause them to be displaced in the image. Registration of subsequent images to the master will be done at a selected sparse array of control points, using either the ground control points or a set of relative control points.

The construction for estimation of effects is given in Figure F-1. From similar triangles,

$$\frac{h}{H - h} = \frac{p}{d}$$ which, since $h \ll H$, can be approximated by:

$$\frac{h}{H} \approx \frac{p}{d} \quad .$$

The relief displacement p is seen to be dependent on the angle of view as represented by the distance d from the nadir to the point in question.

Landsat does not return precisely to the same location in viewing a given WRS, so that two versions of the same scene may be imaged from two vantage points close together but not coincident. This is the normal stereo construction. These are indicated as points 1 and 2 in Figure F-1. Using this construction, the shift R in relief displacement for points at different altitudes is

$$R = D\frac{h}{H} \quad .$$

Note that this shift R is constant at all points in the image, and grows with increase in center separation D. (In stereo parlance, D is the stereo base.) Thus, even though the average ground location of each of a pair of images will be identified using the ephemeris and attitude data, ground altitude deviations will cause individual field boundaries to be displaced. For the range of center separations D to be expected, the amount of shift R in local points may be within the range (say, 0.2 to 1 pixel) which can cause edge pixel effects.

Thus, precision analysis and mapping will require the correction of image data location for all pixels. A candidate source of the required altitude data is the USGS surface altitude digital data, provided that it can be registered to Landsat to the required accuracy.

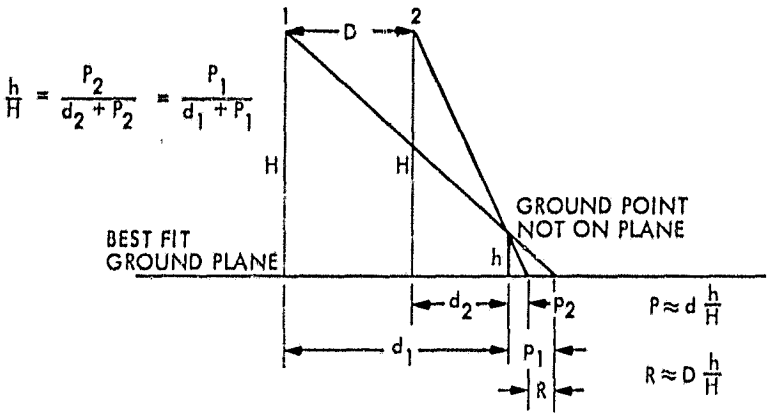

Figure F-1 Construction for Relief Displacement (p) and Relief Displacement Shift (R)

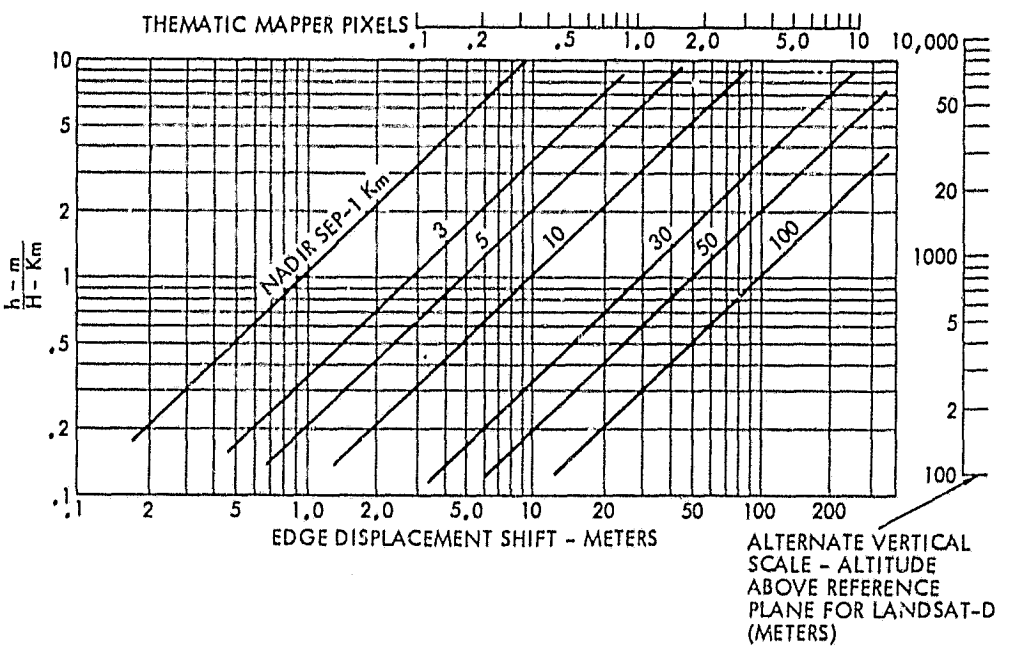

Figure F-2 Relief Displacement Shift R as a Function of Nadir Separation for Varying Altitude of the Ground above a Reference Plane